MOLECULAR AND CELLULAR BIOLOGY, Mar. 2007, p. 1730–1744 Vol. 27, No. 5
0270-7306/07/$08.00+0 doi:10.1128/MCB.01579-06

Reduced Levels of ATF-2 Predispose Mice to Mammary Tumors†▽

Toshio Maekawa,[1] Toshie Shinagawa,[1] Yuji Sano,[1] Takahiko Sakuma,[2] Shintaro Nomura,[2] Koichi Nagasaki,[3] Yoshio Miki,[3] Fumiko Saito-Ohara,[4] Johji Inazawa,[4] Takashi Kohno,[5] Jun Yokota,[5] and Shunsuke Ishii[1]*

Laboratory of Molecular Genetics, RIKEN Tsukuba Institute, 3-1-1 Koyadai, Tsukuba, Ibaraki 305-0074, Japan[1]; Department of Pathology, Graduate School of Medicine, Osaka University, 2-2 Yamada-oka, Suita, Osaka 565-0871, Japan[2]; The Genome Center of the Japanese Foundation for Cancer Research, Kami-ikebukuro, Toshima-ku, Tokyo 170-8455, Japan[3]; Department of Molecular Cytogenetics, Medical Research Institute, Tokyo Medical and Dental University, 1-5-45 Yushima, Bunkyo-ku, Tokyo 113-8510, Japan[4]; and Biology Division, National Cancer Center Research Institute, 1-1 Tsukiji 5-chome, Chuo-ku, Tokyo 104-0045, Japan[5]

Received 24 August 2006/Returned for modification 13 October 2006/Accepted 10 December 2006

Transcription factor ATF-2 is a nuclear target of stress-activated protein kinases, such as p38, which are activated by various extracellular stresses, including UV light. Here, we show that ATF-2 plays a critical role in hypoxia- and high-cell-density-induced apoptosis and the development of mammary tumors. Compared to wild-type cells, *Atf-2*$^{-/-}$ mouse embryonic fibroblasts (MEFs) were more resistant to hypoxia- and anisomycin-induced apoptosis but remained equally susceptible to other stresses, including UV. *Atf-2*$^{-/-}$ and *Atf-2*$^{+/-}$ MEFs could not express a group of genes, such as *Gadd45*α, whose overexpression can induce apoptosis, in response to hypoxia. *Atf-2*$^{-/-}$ MEFs also had a higher saturation density than wild-type cells and expressed lower levels of *Maspin*, the breast cancer tumor suppressor, which is also known to enhance cellular sensitivity to apoptotic stimuli. *Atf-2*$^{-/-}$ MEFs underwent a lower degree of apoptosis at high cell density than wild-type cells. *Atf-2*$^{+/-}$ mice were highly prone to mammary tumors that expressed reduced levels of *Gadd45*α and *Maspin*. The *ATF-2* mRNA levels in human breast cancers were lower than those in normal breast tissue. Thus, ATF-2 acts as a tumor susceptibility gene of mammary tumors, at least partly, by activating a group of target genes, including *Maspin* and *Gadd45*α.

The ATF family of transcription factors (13), which have the b-ZIP-type DNA-binding domain, contains multiple members that play diverse roles (24, 27, 39, 53). ATF-2, one member of the ATF family (28), can form either homodimers or heterodimers with c-Jun and subsequently bind to the cyclic AMP response element (CRE) (5′-TGACGTCA-3′) (12, 29, 48). Heterodimerization of ATF-2 with Jun appears to be crucial for at least some of its functions; for instance, the oncogenic activity of ATF2 in chicken cells critically depends on its ability to dimerize with c-Jun (16). The c-Jun/ATF-2 heterodimers are more potent transcriptional activators for the minimal promoters containing CRE than ATF-2 homodimers (3, 16, 50). The target genes of c-Jun/ATF-2 heterodimers, which are implicated in growth control, include c-*jun* itself, cyclin D1, cyclin A, and beta interferon (2, 8, 31, 42).

The ATF-2 subfamily includes ATF-7 (originally called ATF-a) and CRE-BPa. All three of these members bear the *trans*-activation domain in their N-terminal regions (10, 35), which consists of two subdomains, namely, the N-terminal subdomain containing the well-known zinc finger motif and the C-terminal subdomain containing the SAPK phosphorylation sites targeted by stress-activated protein kinases (SAPKs) (33). The latter subdomain has a highly flexible and disordered structure. SAPKs, such as JNK (c-Jun N-terminal protein kinase) and p38, phosphorylate ATF-2 at Thr-69 and Thr-71 in the C-terminal subdomain and thereby enhance its *trans*-activating capacity (11, 26, 49). SAPKs are activated by various extracellular stresses, such as UV, osmotic stress, hypoxia, and inflammatory cytokines (6, 32). Activation of ATF-2 by p38/JNK is thought to play a role in apoptosis (11, 38).

Phosphorylation of ATF-2 by p38 is also induced by the transforming growth factor β-TAK1 pathway, while ATF-2 interacts with Smad3/4 to synergistically activate transcription (40). Thus, ATF-2 plays an important role in transforming growth factor β signaling by acting as a common nuclear target of both the Smad and TAK1 pathways. In fibroblasts, ATF-2 is also activated by insulin, epidermal growth factor (EGF), and serum via a two-step mechanism involving two distinct Ras effector pathways, the Raf-MEK-ERK and Ral-RalGDS-Src-p38 pathways (36). Serum stimulation leads to induction of ATF-3 gene transcription by activation of ATF-2 via these Ras effector pathways (47). Although CBP binds to ATF-2 and stimulates ATF-2 activity (41), the interaction between CBP and ATF-2 is phosphorylation independent, and the mechanism whereby SAPK-induced phosphorylation stimulates ATF-2 activity remains unknown. Recently, the protein kinase ATM was shown to phosphorylate ATF-2 on Ser-490 and Ser-498 following ionizing radiation, which resulted in its rapid colocalization with γ-H2AX into ionizing radiation-induced foci (4). In this case, a role for ATF-2 in the DNA damage

* Corresponding author. Mailing address: Laboratory of Molecular Genetics, RIKEN Tsukuba Institute, 3-1-1 Koyadai, Tsukuba, Ibaraki 305-0074, Japan. Phone: 81-29-836-9031. Fax: 81-29-836-9031. E-mail: sishii@rtc.riken.jp.

† Supplemental material for this article may be found at http://mcb.asm.org.

▽ Published ahead of print on 22 December 2006.

response appears to be uncoupled from its transcriptional activity.

ATF-2 is ubiquitously expressed, with the highest level of expression being observed in the brain (45). Hypomorphic *Atf-2* mutant mice, which still express an alternatively spliced ATF-2 protein, exhibit lower postnatal viability and growth, defects in endochondrial ossification, and a reduced number of cerebellar Purkinje cells (39). Null *Atf-2* mutant mice die shortly after birth (27). In the mutant embryos, hypoxia occurs and was suggested to lead to strong gasping respiration with consequent aspiration of the amniotic fluid containing meconium. Impaired development of cytotrophoblast cells and a decreased level of expression of the platelet-derived growth factor receptor α, which is one of the ATF-2 target genes, were observed in the mutant placenta, suggesting a possible linkage of these events. However, the precise normal physiological role of ATF-2 remains elusive.

MATERIALS AND METHODS

Detection of apoptotic cells. Cells (3×10^5 per 60-mm dish) were cultured in Dulbecco's modified Eagle's medium (DMEM) supplemented with 10% fetal bovine serum (FBS), and apoptotic cells were detected by the terminal deoxynucleotidyltransferase-mediated dUTP-biotin nick end labeling (TUNEL) method using the Deadend Colorimetric Apoptosis Detection System (Promega). Hypoxic conditions were introduced using the oxygen absorber Anaero Pack (Mitsubishi Gas Chemical). Conditions of other stresses were introduced as follows: methyl methanesulfonate (MMS) (1 mM for 20 h), anisomycin (AM) (5 μg/ml for 12 h), and UV light (50 J/m^2 20 h before TUNEL assays). The average of three independent experiments was obtained from three different mouse embryonic fibroblast (MEF) preparations. To examine *GADD45*α-induced apoptosis, *p53*$^{-/-}$ MEFs were transfected with 3 μg of pact-GADD45-IRES-EGFP or pact-IRES-EGFP plasmid using Lipofectamine Plus (Invitrogen). After 40 h, dead cells were detected by TUNEL using an ApopTagRed in situ apoptosis detection kit (Intergen). To investigate apoptosis at the saturated cell density, MEFs and SK-BR-3 cells were cultivated to confluence, and apoptotic cells were detected by the TUNEL method.

DNA microarrays. MEFs were mixed with TRIzol reagent (Invitrogen), and biotin-labeled RNAs for GeneChip analysis were prepared according to the protocol available on the Affymetrix website. The Mouse Genome Array, containing more than 12,422 probe sets (Affymetrix; U74Av2 DNA Chip), was used for the analysis.

Northern analysis. RNA was prepared from MEFs and MEF-derived immortalized cell lines using the NIH 3T3 protocol. Cells were seeded at 2×10^6 per 10-cm dish and stimulated with either hypoxic conditions (24 h), AM (5 μg/ml for 4 h), MMS (1 mM for 4 h), or UV light (50 J/m^2 4 h before cells were harvested). Twenty micrograms of total RNA was then electrophoresed in a 1.2% agarose formaldehyde gel and then transferred onto a nitrocellulose membrane (S&S). The blot was hybridized with a ^{32}P-labeled mouse *Gadd45*α 500-bp cDNA probe that covered the entire protein-coding region. The signals from Northern blotting were quantitated by using Image Analyzer (Fuji).

Reporter assays. To investigate the responsiveness of the *Gadd45*α promoter to the transcriptional activator p53, *p53*$^{-/-}$ MEF-derived immortalized cells were transfected with the *Gadd45*α promoter-Luci reporter (0.2 μg), in which the human *GADD45*α promoter region (nucleotides −2256 to + 287) was linked to the luciferase gene, the p53 expression plasmid (pact-p53), or the control empty vector (5 μg), and the internal control pRL-SV40 (10 ng; Promega) using Lipofectamine Plus (Invitrogen). The transfected cells were irradiated by UV light (20 J/m^2) 24 h before being harvested. Forty hours after transfection, luciferase activity was measured by using the Dual-luciferase reporter assay system (Promega). To examine the c-Jun-dependent *trans*-activation, *p53*$^{-/-}$ MEF-derived immortalized cells were transfected with the chloramphenicol acetyltransferase (CAT) reporter (pTRE-TK-CAT; 1 μg), in which the herpesvirus thymidine kinase gene promoter was linked to four tandem repeats of the TRE (tetradecanoyl phorbol acetate response element) from the collagenase gene promoter, the c-Jun expression plasmid (pRSV-c-Jun), or the control empty vector (4 μg), and the internal control pCMV-β-gal (2 μg) using the $CaPO_4$ method. CAT activity was measured 40 h after transfection.

Western blotting. To detect ATF-2 and c-Jun proteins in MEFs, nuclear extracts were prepared from MEFs as described by Dignam et al. (7) and used for Western blotting. To detect ATF-2 and Maspin proteins in tumors, whole-cell extracts were prepared from tumors by using RIPA buffer (50 mM Tris-HCl, pH 7.8, 150 mM NaCl, 1% Triton X-100, 1% deoxycholate, 0.1% sodium dodecyl sulfate, 1% Trasylol), and used for Western blotting. Anti-ATF-2 (Santa Cruz C-19), anti-c-Jun (Santa Cruz H-79), and anti-Maspin (Santa Cruz C-20) antibodies were used.

ChIP assays. Chromatin immunoprecipitation (ChIP) assays were carried out essentially as described previously (18) with minor modifications. Cells were treated under hypoxic conditions for 30 h. Immunoprecipitations were performed with either rabbit anti-ATF2 (Santa Cruz C-19) or rabbit normal immunoglobulin G (IgG). The primers for the amplification of the *Gadd45*α promoter region were as follows: forward (5′-TCTGGGTGTCAACGTCTGCTAA-3′), reverse (5′-CAGGTCCAGCTTCATTTGCA-3′), and TaqMan probe (5′-6-carboxyfluorescein [FAM]-TTGCATAACCCAATGGCCTGACTGC-6-carboxytetramethylrhodamine [TAMRA]-3′).

RT-PCR. To measure the levels of Arnt, DecxE1a (branched-chain α ketoacid decarboxylase E1a), and Cyt-β-actin mRNAs, cells were treated under hypoxic conditions for 24 h, and total RNA was prepared. Real-time reverse transcription (RT)-PCR was performed by using the ABI 9700 Real-Time PCR Instrument and the SYBR Green qRT-PCR Kit (QIAGEN) according to the supplier's protocol. The primers used were as follows: Arnt, 5′-CTTGGCTCTGTGAAGGAAGG-3′ and 5′-GTCATCATCTGGGAGGGAGA-3′; DecxE1a, 5′-AGAACCAGCCCTTCCTCATT-3′ and 5′-GGTCCTGCTTGTCCCAGTAA-3′; and Cyt-β-actin, 5′-GCGCAAGTACTCTGTGTGGA-3′ and 5′-ACATCTGCTGGAAGGTGGAC-3′.

Maspin and *Gadd45*α mRNA levels were determined by real-time RT-PCR by using the ABI 9700 Real-Time PCR Instrument and the QuantiTect Probe RT-PCR Kit (QIAGEN) according to the manufacturers' instructions. The PCR conditions were 50°C for 30 min, 95°C for 10 min, and 40 cycles of 95°C for 15 s and 60°C for 1 min. The oligonucleotide primers and probe used were as follows: *Maspin*, 5′-GGAAGTACCATTGGCACAAACTG-3′, 5′-GAGCAGCACATTGGGAACCT-3′, and 5′-FAM-AGCCCACATCAGCTATCGTTCGTCCA-TAMRA-3′; mouse *Gadd45*α, 5′-GCTGGCTGCTGACGAAGAC-3′, 5′-CGGATGAGGGTGAAATGGAT-3′, and 5′-FAM-ACGACCGGGATGTGGCTCTG-TAMRA-3′; and human *Gadd45*α, 5′-GGATGCCCTGGAGGAAGTG-3′, 5′-TCGTACACCCCGACAGTGATC-3′, and 5′-FAM-TCAGCAAAGCCCTGAGTCAGCGC-TAMRA-3′.

To determine the mRNA levels in the mammary tumors of *Atf-2*$^{+/-}$ mice, total RNA was isolated from mouse tumor tissues and normal mammary glands using Isogen (Nippon Gene). To separate the mammary glands from surrounding fat cells, the mammary glands were minced and dissociated for 3 h at 37°C in M199 medium containing 420 μg/ml collagenase and 2.1 mg/ml hyaluronidase. The cells were washed twice with Waymouth's MB 752-1 medium and cultured overnight in the same medium supplemented with 10% FBS. Only cells from mammary glands that attached were collected and further analyzed. RT-PCR was performed using 0.5 μg of total RNA and the Superscript One-Step RT-PCR System (Invitrogen). After 30 min of incubation at 50°C, cDNAs were amplified with 22 cycles of PCR under the following conditions: 94°C for 15 s, 55°C for 30 s, and 72°C for 90 s. The following primers were used for PCR: *Atf-2*, 5′-ACCAATGGTGATACTGTAAAAGGCC-3′ and 5′-CAGAAAGGTCTTCTGAACTGTCATC-3′; *p53*, 5′-CCGAGGCCGGCTCTGAGTATACCACCATC-3′ and 5′-CTCATTCAGCTCCCGGAACATCTCGAAGCG-3′; *Gadd45*α, 5′-GAGGGACTCGCACTTGCAATATGAC-3′ and 5′-CAGGATGTTGATGTCGTTCTCGCAG-3′; *Gapdh*, 5′-TTCCAGTATGACTCCACTCA-3′ and 5′-ATCACGCCACAGCTTTCCAG-3′; and *Maspin*, 5′-TAAATAAATGGATGGTCAGCATTG-3′ and 5′-AGACCAAAATCCTTGTGGTTAATG-3′.

To determine the human *ATF-2* mRNA levels, breast cancers and normal epithelial cells were obtained using the laser capture microdissection technique. The two samples contained comparable levels of epithelial cells. Total RNA was isolated from individual frozen tumors, from normal epithelial cells, and from cell lines using RNeasy (QIAGEN). One-tube real-time RT-PCR was performed by using the QuantiTect SYBR Green RT-PCR Kit (QIAGEN) according to the manufacturer's instructions. Expression of *ATF2* in relation to the *TFR* gene was determined by real-time PCR by using the SYBR Green assay with an ABI Prism 7900 (PE Applied Biosystems). The following primers were used: *ATF-2*, 5′-CGACAAAAAAGGAAAGTCTGGGTT-3′ and 5′-GCTCTGTACTCTGGTCCGCCA-3′; *TFR*, 5′-GCAAAATGTGAAGCATCCGGT-3′ and 5′-GCCACTGTAAACTCAGGCCCA-3′.

Analysis of growth properties of MEFs and human mammary epithelial cells (HMEC). MEFs were isolated from embryos at 14.5 days postcoitus. For growth curves, the cells were grown from a starting density of 2.5×10^4 cells per well in

24-well plates in DMEM supplemented with 10% FBS. To determine the focus-formation efficiency, cells were seeded onto 6-cm dishes at 100 cells/dish and incubated in DMEM plus 10% FBS. After 12 days, the samples were stained with Giemsa, and the number of visible foci was scored. For colony formation assays, MEFs were infected with murine leukemia virus carrying v-K-*ras* (multiplicity of infection, 1). After 48 h, 3×10^4 cells were suspended in 1.3% methylcellulose gel dissolved in culture medium and laid onto an agarose bed composed of 0.53% agarose in culture medium. Colonies were scored 3 weeks after being plated. For growth curves, focus formation assays, and colony formation assays, three independent experiments were carried out using three different MEF preparations. To reexpress ATF-2, the retrovirus expression vectors for *ATF-2* were constructed by using the retroviral vector carrying the puromycin resistance marker and viruses were prepared as described previously (44).

To test the tumorigenicity of the cell clones, nude mice (BALB/c nu/nu; Clea Japan Inc.) were injected subcutaneously at 12 sites (2 sites per mouse) with 1×10^6 or 2×10^6 cells resuspended in 100 μl of phosphate-buffered saline. The sizes and weights of the resulting tumors were measured 10 days (for MEFs), 14 days (for MEFs, to examine the effect of *Maspin*), 16 days (for NIH 3T3 cells, to examine the effect of *Maspin*), 12 days (for MEFs, to examine the effect of *Gadd45*α), or 21 days (for MCF-12A cells) after injection. The retrovirus expression vectors for *Maspin* or *Gadd45*α were constructed by using the retroviral vector carrying the puromycin resistance marker, and viruses were prepared as described previously (44). *Atf-2*$^{-/-}$ MEF-derived cell clones expressing v-K-*ras* were infected with the virus, and the puromycin-resistant cell pool was used for injection into nude mice. To test the effect of *Maspin* on Ras-induced tumor formation, NIH 3T3-R21 cells that were transformed by activated K-*ras* were infected with the Maspin-expressing virus, and the puromycin-resistant cell pool was used for injection into nude mice.

To decrease *ATF-2* mRNA levels by RNA interference, the pDECAP-ATF-2 construct containing the inverted sequence of the mouse *Atf-2* protein-coding region that corresponded to amino acids 166 to 362 was constructed using the pDECAP vector (43). MCF12A cells were transfected with pDECAP-ATF-2 or the empty vector, and the tranformants were isolated. To overexpress ATF-2, SK-BR3 cells were transfected with the *ATF-2* expression vector containing the β-actin promoter, insulator, and neomycin selection marker (pact-ATF-2-Ins) or the control empty vector, and clones were isolated. Their growth properties were analyzed as described above.

Mice, histological analysis, and immunohistochemistry. All *Atf-2*$^{+/-}$ and control wild-type mice analyzed had a 75% BALB/c, 12.5% C57BL/6J, and 12.5% CBA genetic background. Tissues were fixed in 4% paraformaldehyde, dehydrated, and embedded in paraffin. Sections (5 μm) were stained with hematoxylin and eosin according to standard procedures. The histological assessment of tumors was performed according to the WHO classification. Frozen sections (10 μm) were used for immunohistochemistry. For indirect immunofluorescent staining, anti-ATF-2 and anti-GADD45α (N96 and H-165, respectively, from Santa Cruz) were used. The frozen sections were washed twice with Tris-buffered saline buffer (144 mM NaCl, 10 mM Tris-HCl, pH 7.6) and incubated overnight at 4°C with primary antibody. Biotin-conjugated anti-rabbit IgG antibody served as the secondary antibody and was incubated at room temperature for 2 h and further incubated with fluorescein isothiocyanate-streptavidin at room temperature for 1 h.

CGH. To determine genomic changes, we performed comparative genomic hybridization (CGH) using fluorochrome-conjugated DNA as previously described (9). Briefly, tumor and normal DNAs were labeled by nick translation using Spectrum Green-dUTP and Spectrum Orange-dUTP (Vysis), respectively. Labeled tumor and normal DNAs (250 ng each), together with 10 μg mouse Cot-1 DNA (Gibco-BRL), were denatured and hybridized to normal mouse metaphase chromosome spreads that were prepared from fetal mouse skin fibroblasts. Slides were washed and counterstained with 4′,6′-diamidino-2-phenylindole (DAPI). Relative changes in the copy numbers of DNA sequences were analyzed in at least five cells per tumor by using a digital image analysis system (Quips-XL software; Vysis). Shifts in CGH profiles were rated as gains or losses if they reached at least the 1.2 and 0.8 thresholds, as described elsewhere (52).

Statistical analysis. Some data are presented as means ± standard errors of the mean (SEM). The *P* values were obtained by Fisher's protected least significant difference PLSD test.

RESULTS

ATF-2 is critical for hypoxia-induced apoptosis. Since ATF-2 is a nuclear target of p38/JNK, which is involved in stress-induced apoptosis, we examined the rates of cell death induced by various treatments of wild-type and *Atf-2*$^{-/-}$ MEFs. *Atf-2*$^{-/-}$ MEFs were slightly but significantly more resistant to hypoxia-induced apoptosis than wild-type cells (statistical analysis indicated a *P* value of <0.01) (Fig. 1A, left). Moreover, although most of the wild-type cells that survived the hypoxia were rounded, the *Atf-2*$^{-/-}$ cells exhibited normal morphology (Fig. 1A, middle). The resistance of *Atf-2*$^{-/-}$ cells to hypoxia-induced apoptosis was more significant when *Atf-2*$^{-/-}$ *p53*$^{-/-}$ MEFs were compared to *p53*$^{-/-}$ MEFs (Fig. 1A, right). By the fourth day of hypoxic conditions, almost no apoptotic cells were detected in the *Atf-2*$^{-/-}$ *p53*$^{-/-}$ MEFs, whereas about 70% of *p53*$^{-/-}$ cells were apoptotic. These results suggest that some target genes of ATF-2 and p53 that are induced by hypoxic stress may overlap. In contrast to hypoxia, no differences were noted between the *Atf-2*$^{-/-}$ *p53*$^{-/-}$ and *p53*$^{-/-}$ cells in the degrees of apoptosis induced by MMS or UV light (Fig. 1B). *Atf-2*$^{-/-}$ *p53*$^{-/-}$ MEFs were slightly but significantly more resistant to AM-induced apoptosis than *p53*$^{-/-}$ cells (statistical analysis indicated a *P* value of <0.01). Thus, ATF-2 is critical for the apoptosis induced by specific stress, such as hypoxia and AM.

A group of genes, such as *Gadd45*α, are regulated by ATF-2 upon hypoxic stress. To identify the ATF-2 target genes that participate in hypoxia-induced apoptosis, we performed DNA array analysis using RNAs from *p53*$^{-/-}$ and *Atf-2*$^{-/-}$ *p53*$^{-/-}$ MEFs after 2 days of hypoxic treatment. The loss of *Atf-2* caused greater than threefold down-regulation of 978 genes (Fig. 1C). When RNAs from *p53*$^{-/-}$ MEFs treated with and without hypoxic stress were evaluated by DNA array analysis, 126 genes were up-regulated more than threefold by hypoxic stress (Fig. 1C). A comparison of the 978 down-regulated and the 126 up-regulated genes revealed 39 shared genes. Thus, of all the hypoxia-inducible genes, ATF-2 appears to regulate ~30% (39/126) of them, suggesting that ATF-2 is a major inducer of gene expression during hypoxic stress. The remaining 939 genes were down-regulated by a loss of ATF-2 during hypoxic stress.

Of these ATF-2 target genes, the functions of 21 genes are known (Fig. 1C), and most of them have been reported to be involved in the regulation of apoptosis. To more precisely analyze the ATF-2-dependent transcriptional regulation of these genes, we focused on the *Gadd45*α gene, which has been clearly demonstrated to be a regulator of apoptosis (46). In fact, we found that *GADD45*α overexpression induced apoptosis in *p53*$^{-/-}$ MEFs (Fig. 1D). However, in earlier studies, *Gadd45*α mutant mice did not exhibit the defects in hypoxia-induced apoptosis (15), suggesting that multiple ATF-2 target genes cooperatively contribute to the hypoxia-induced apoptosis and that a loss of one gene among them, such as *Gadd45*α, is not sufficient to abrogate the hypoxia-induced apoptosis.

When we examined the *Gadd45*α expression levels induced by various stresses in wild-type, *Atf-2*$^{+/-}$, and *Atf-2*$^{-/-}$ MEFs, there were almost no differences in the degrees of induction of *Gadd45*α expression among them (data not shown). This is consistent with our observation that similar numbers of apoptotic cells were detected in wild-type and *Atf-2*$^{-/-}$ MEFs after hypoxic stress (Fig. 1A, left). However, we found a clear difference between the degrees of *Gadd45*α induction in wild-

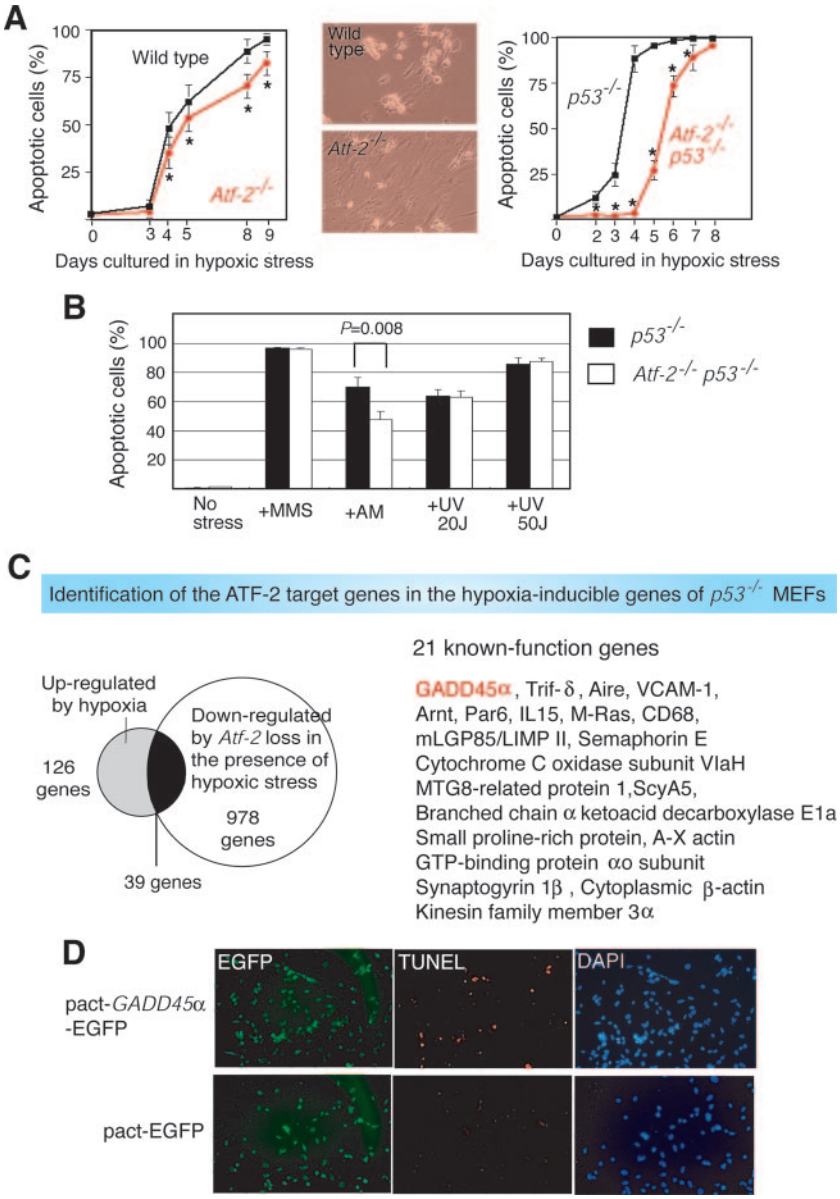

FIG. 1. Role of ATF-2 in hypoxia-induced apoptosis. (A) Deletion of ATF-2 in MEFs confers resistance to hypoxia-induced apoptosis (left), and this is enhanced in the *p53*$^{-/-}$ background (right). MEFs were prepared from the indicated genotypes, and apoptosis was induced by hypoxia. Apoptotic cells were detected by TUNEL labeling. The averages of three measurements are shown with their SEM. *, $P < 0.01$. The morphologies of the *Atf-2*$^{-/-}$ and wild-type cells on day 9 are shown (middle). (B) Effects of loss of *Atf-2* on the apoptosis induced by various stresses. *p53*$^{-/-}$ and *Atf-2*$^{-/-}$ *p53*$^{-/-}$ MEFs were treated with various stresses, and apoptotic cells were detected by TUNEL labeling. The averages of three measurements are shown with their SEM. (C) Identification of *Gadd45*α as an ATF-2 target gene that is induced by hypoxia. RNAs from *p53*$^{-/-}$ and *Atf-2*$^{-/-}$ *p53*$^{-/-}$ MEFs that had been exposed to hypoxic stress for 2 days were subjected to DNA array analysis; 978 genes were down-regulated more than threefold by the loss of *Atf-2*. DNA array analysis was also performed on RNAs from *p53*$^{-/-}$ MEFs with or without hypoxia treatment, which revealed that 126 genes were up-regulated more than threefold by hypoxia. Comparison of the 978 down-regulated and 126 up-regulated genes indicated that 39 genes were common to both groups. Of these 39, the functions of 21 (including *Gadd45*α) are known. These genes are listed on the right. (D) Overexpression of *GADD45*α in MEFs induces apoptosis. *p53*$^{-/-}$ MEFs were transfected with a plasmid expressing both *GADD45*α and enhanced green fluorescent protein (EGFP) or EGFP alone, and apoptotic cells were detected by TUNEL labeling. All cells were detected by DAPI staining, while the transfected cells were marked by EGFP expression.

type and *Atf-2*$^{-/-}$ cells immortalized from MEFs (Fig. 2A). The loss of *p53* function in immortalized cells may be involved, because spontaneously immortalized cell lines derived from primary MEFs have been shown to exhibit either *p53* or *Arf* loss of function with high frequency (20, 21). Indeed, the role of ATF-2 in hypoxia-induced apoptosis was more clear in p53$^{-/-}$ cells than in p53$^{+/+}$ cells (Fig. 1A).

In previous reports, p53 induced *Gadd45*α transcription (19), and our reporter assays using the *Gadd45*α promoter-luciferase reporter confirmed that p53 activates the *Gadd45*α

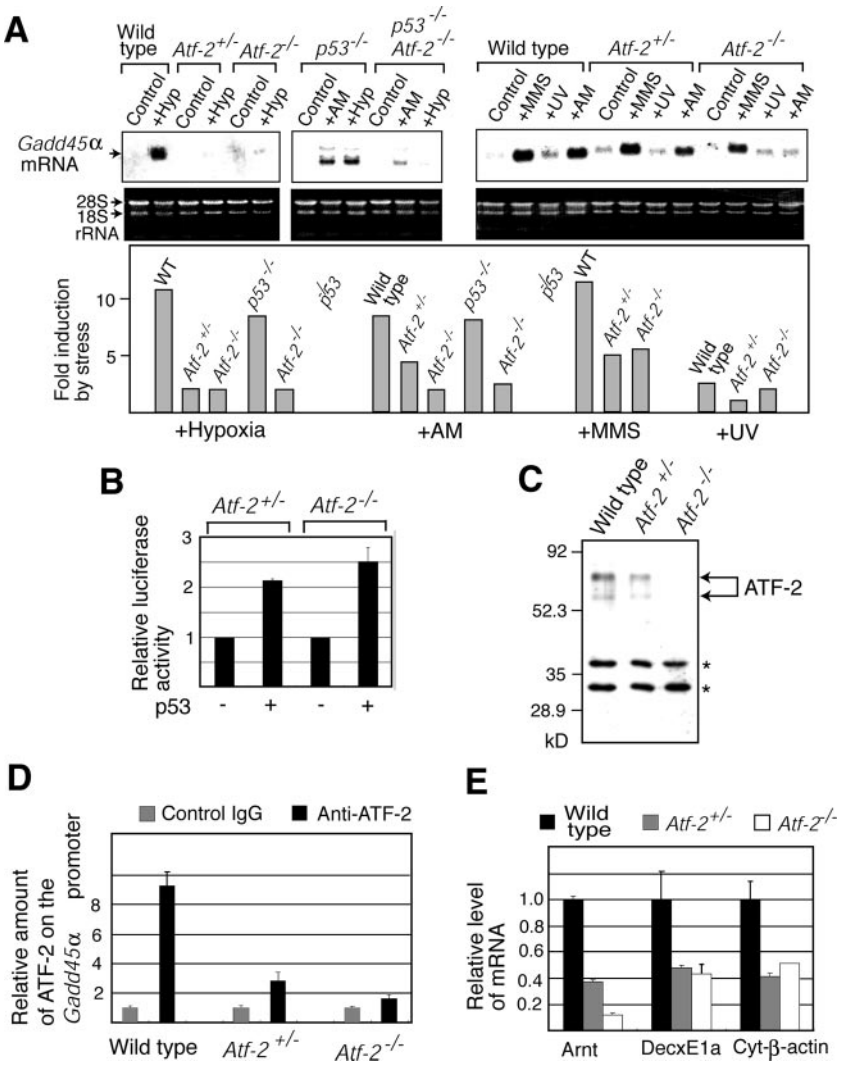

FIG. 2. Loss of one allele of *Atf-2* impairs the induction of *Gadd45*α upon hypoxic (Hyp) stress. (A) Northern blotting of *Gadd45*α mRNA. RNAs were isolated from wild-type (WT), *Atf-2*$^{+/-}$, and *Atf-2*$^{-/-}$ cells immortalized from MEFs and *p53*$^{-/-}$ and *p53*$^{-/-}$ *Atf-2*$^{-/-}$ MEFs that were subjected to the stress indicated above each lane, and expression of *Gadd45*α mRNA was analyzed by Northern blotting. The degree of induction is shown below in the bar graphs. (B) p53 responsiveness of the *Gadd45*α gene promoter. The *Gadd45*α promoter-luciferase reporter was cotransfected into *Atf-2*$^{+/-}$ or *Atf-2*$^{-/-}$ cells immortalized from MEFs with or without a p53 expression vector. Transfected cells were irradiated by UV, and luciferase activity was measured. The averages of relative degrees of activation by p53 ($n = 3$) are shown with SEM. (C) Levels of ATF-2 protein. Whole-cell extracts from wild-type, *Atf-2*$^{+/-}$, and *Atf-2*$^{-/-}$ cells immortalized from MEFs were used for Western blotting with the anti-ATF-2 antibody. The bands indicated by asterisks are nonspecific signals. (D) ChIP assays. Wild-type, *Atf-2*$^{+/-}$, and *Atf-2*$^{-/-}$ cells immortalized from MEFs were subjected to hypoxic stress for 30 h. Soluble chromatin was prepared and immunoprecipitated with anti-ATF-2 or control IgG. The final DNA extraction was amplified by real-time PCR using the primers that cover the *Gadd45*α promoter region. The relative densities of bands are indicated. (E) Expression levels of ATF-2 target genes. Wild-type, *Atf-2*$^{+/-}$, and *Atf-2*$^{-/-}$ cells immortalized from MEFs were subjected to hypoxic stress, and total RNA was prepared. The levels of three ATF-2 target genes (Arnt, DecxE1a, and Cyt-β-actin), which were identified using DNA array analysis in panel C, were measured by real-time RT-PCR. The levels (mean plus SEM; $n = 3$) are shown relative to the levels of wild-type cells.

promoter upon UV irradiation in *Atf-2*$^{+/-}$ and *Atf-2*$^{-/-}$ cells, suggesting that p53 can function in these cells (Fig. 2B). In wild-type MEFs, *Gadd45*α mRNA levels were increased 10.5- and 8-fold by hypoxia and AM, respectively, while a similar degree of induction was observed in *p53*$^{-/-}$ MEFs (Fig. 2A). However, this parameter was elevated only 2- to 2.5-fold in both *Atf-2*$^{-/-}$ and *Atf-2*$^{-/-}$ *p53*$^{-/-}$ cells, indicating that ATF-2 plays a role in the p53-independent induction of *Gadd45*α. This is consistent with our observation that ATF-2 is recruited to the sites in the *GADD45*α promoter, which are different from the p53-binding sites (unpublished results). The lack of an effect of p53 mutation on the hypoxia-dependent induction of *Gadd45*α suggests that ATF-2 can mediate the induction of *Gadd45*α upon hypoxic stress in *p53*$^{-/-}$ cells.

In wild-type cells, MMS and UV irradiation treatment increased the *Gadd45*α mRNA levels by 11- and 2.5-fold, respectively (Fig. 2A). In contrast to the effects of hypoxia or AM, MMS further increased *Gadd45*α mRNA levels by fivefold in *Atf-2*$^{-/-}$ cells. Deletion of *Atf-2* had little effect on UV light-induced *Gadd45*α transcription. This is consistent with our

observations that *Atf-2*$^{-/-}$ MEFs are not resistant to MMS- or UV light-induced apoptosis.

Down-regulation of hypoxia-induced *Gadd45*α expression by loss of one copy of *Atf-2*. Hypoxia increased *Gadd45*α mRNA expression in *Atf-2*$^{-/-}$ cells and in *Atf-2*$^{+/-}$ cells only twofold (Fig. 2A). Western blotting analysis indicated that the two forms of ATF-2 protein, consisting of 70- and 62-kDa polypeptides, were expressed in wild-type MEFs (Fig. 2C). These two forms had been detected previously in brain extracts (27) and may be generated by alternative splicing, as reported previously (17). In *Atf-2*$^{+/-}$ cells, the amounts of both forms of ATF-2 were about half of that in wild-type cells, while no ATF-2 was detected in *Atf-2*$^{-/-}$ cells. ChIP assays showed an ~80% reduction in the amount of ATF-2 bound to the *Gadd45*α promoter in *Atf-2*$^{+/-}$ cells compared to wild-type cells (Fig. 2D). These results suggest that the loss of even one copy of *Atf-2* reduces the amount of ATF-2 bound to the *Gadd45*α promoter and impairs hypoxia-induced *Gadd45*α transcription. Perhaps the rapid induction of *Gadd45*α that occurs with hypoxic stress requires large amounts of ATF-2; a 50% reduction in ATF-2 levels may cause the inefficient induction of *Gadd45*α. To further confirm whether loss of one copy of *Atf-2* reduces the expression levels of other ATF-2 target genes upon hypoxic stress, we examined the levels of three ATF-2 target genes identified above. The level of these genes, encoding Arnt, DecxE1a, and cytoplasmic β-actin, were significantly reduced in *Atf-2*$^{+/-}$ cells compared to wild-type cells (Fig. 2E). Thus, loss of one copy of *Atf-2* reduces the levels of multiple hypoxia-inducible genes that are regulated by ATF-2.

Growth properties of *Atf-2*-deficient cells. When grown at low densities, wild-type, *Atf-2*$^{+/-}$, and *Atf-2*$^{-/-}$ MEFs were morphologically indistinguishable and had no significant differences in their growth rates (Fig. 3A) and similar numbers of cells in each phase of the cell cycle (data not shown). However, *Atf-2*$^{+/-}$ and *Atf-2*$^{-/-}$ MEF monolayers reached 5% and 20% higher cell densities, respectively, than wild-type MEFs (statistical analysis indicated a P value of <0.01). Since ATF-2 is involved in stress-induced apoptosis, the higher cell densities achieved by *Atf-2*$^{+/-}$ and *Atf-2*$^{-/-}$ MEFs may indicate that the apoptosis normally induced by high cell density has been abrogated. In fact, when cells reached saturation density, 3.7% and 2.8% of wild-type and *Atf-2*$^{+/-}$ MEFs were apoptotic, respectively, whereas apoptotic *Atf-2*$^{-/-}$ MEFs were only 1.2% (Fig. 3B).

An examination of the transformation capacity showed that *Atf-2*$^{+/-}$ and *Atf-2*$^{-/-}$ MEFs generated 24 to 46 and 12 to 34 colonies, respectively, per 10^3 cells in methylcellulose after infection with retrovirus carrying v-K-*ras* (Fig. 3C), whereas wild-type MEFS formed only 1 to 4 colonies (Fig. 3D). Moreover, when colonies were injected into nude mice, both *Atf-2*$^{+/-}$ and *Atf-2*$^{-/-}$ MEFs expressing v-K-*ras* formed tumors, whereas wild-type MEFs did not (Fig. 3E). To further confirm that the growth properties of *Atf-2*$^{+/-}$ and *Atf-2*$^{-/-}$ MEFs were due to decreased levels of ATF-2, we reexpressed ATF-2 in these cells using the ATF-2-expressing retrovirus. Statistical analyses of these results (Fig. 3C to E) indicated that both *Atf-2*$^{+/-}$ and *Atf-2*$^{-/-}$ MEFs apparently have capacities different from those of wild-type cells ($P < 0.05$), whereas there is no clear difference between *Atf-2*$^{+/-}$ and *Atf-2*$^{-/-}$ MEFs ($P =$ 0.20 to 0.66). These results indicate that loss of one or both copies of *Atf-2* facilitates transformation by activated *ras* in cell culture.

To further confirm the role of ATF-2 in the growth properties of MEFs, we reexpressed ATF-2 in *Atf-2*$^{+/-}$ and *Atf-2*$^{-/-}$ MEFs. Both types of MEFs infected with the ATF-2-expressing virus exhibited lower capacities for focus formation following low-density seeding than those infected with the control virus (Fig. 3F). The levels of ATF-2 in *Atf-2*$^{+/-}$ and *Atf-2*$^{-/-}$ cells infected with ATF-2 virus were about 80% and 60% of that in wild-type cells, respectively (Fig. 3G). Reexpression of ATF-2 significantly reduced the colony formation capacities of both types of cells in methylcellulose (Fig. 3H). Incomplete suppression of tumorigenicity by exogenous expression of ATF-2 could be related to some irreversible events occurring during cloning of cell lines, such as chromosome instability (see Fig. 7).

***Maspin* is a target gene of ATF-2.** To identify the ATF-2 target genes involved in apoptosis in the absence of hypoxic stress, RNAs prepared from normally cultured wild-type and *Atf-2*$^{-/-}$ MEFs were subjected to DNA array analysis. The expression levels of only three genes, namely, *Maspin* and two other genes whose functions are unknown, were decreased by more than threefold in *Atf-2*$^{-/-}$ MEFs compared to wild-type cells (Fig. 4A). Maspin, a member of the serine protease inhibitor (serpin) family, was originally identified as a tumor suppressor in human breast cancers (54) and was recently shown to enhance cellular sensitivity to apoptotic stimuli (25). On the other hand, 34 genes, 20 of known function and 14 of unknown function, were up-regulated in *Atf-2*$^{-/-}$ MEFs (see the supplemental material). All of these genes, whose expression levels are down- or up-regulated by a loss of ATF-2, may contribute to the higher-saturation cell density of *Atf-2*$^{-/-}$ MEFs compared to wild-type cells. However, we focused on *Maspin*, since, of these genes, only *Maspin* appeared to be correlated with transformation. *Maspin* mRNA levels in *Atf-2*$^{-/-}$ MEFs were about one-eighth of that in wild-type cells, although no decrease in *Maspin* mRNA was observed in *Atf-2*$^{+/-}$ MEFs (Fig. 4B). Furthermore, reexpression of ATF-2 in *Atf-2*$^{-/-}$ MEFs restored the expression levels of *Maspin* (Fig. 4C). We found that ATF-2 directly binds to its specific site in the *Maspin* promoter and activates transcription (unpublished results).

***Maspin* and *Gadd45*α are involved in the tumorigenicity of *Atf-2*$^{-/-}$ MEFs.** *Atf-2*$^{-/-}$ MEFs expressing v-K-*ras* were infected with a *Maspin*-expressing retrovirus vector and then injected into nude mice. The *Maspin* mRNA levels in the *Maspin* virus-infected cells were about 2.3-fold higher than that in *Atf-2*$^{-/-}$ MEFs but were still only about one-fourth of that in wild-type cells (Fig. 4D). Overexpression of *Maspin* partially but significantly suppressed the size of tumors generated by v-K-*ras*-expressing *Atf-2*$^{-/-}$ MEFs (Fig. 4E). This incomplete suppression of tumorigenicity could be due to the low levels of *Maspin* expression. In related studies, activated Ras-expressing NIH 3T3 cells were infected with the *Maspin*-expressing virus or the control virus and injected into nude mice. Overexpression of *Maspin* did not suppress the size of tumors (Fig. 4F), indicating that *Maspin* does not affect Ras-induced transformation. We also examined the effect of overexpression of *Gadd45*α on the tumorigenicity of *Atf-2*$^{-/-}$ MEFs expressing

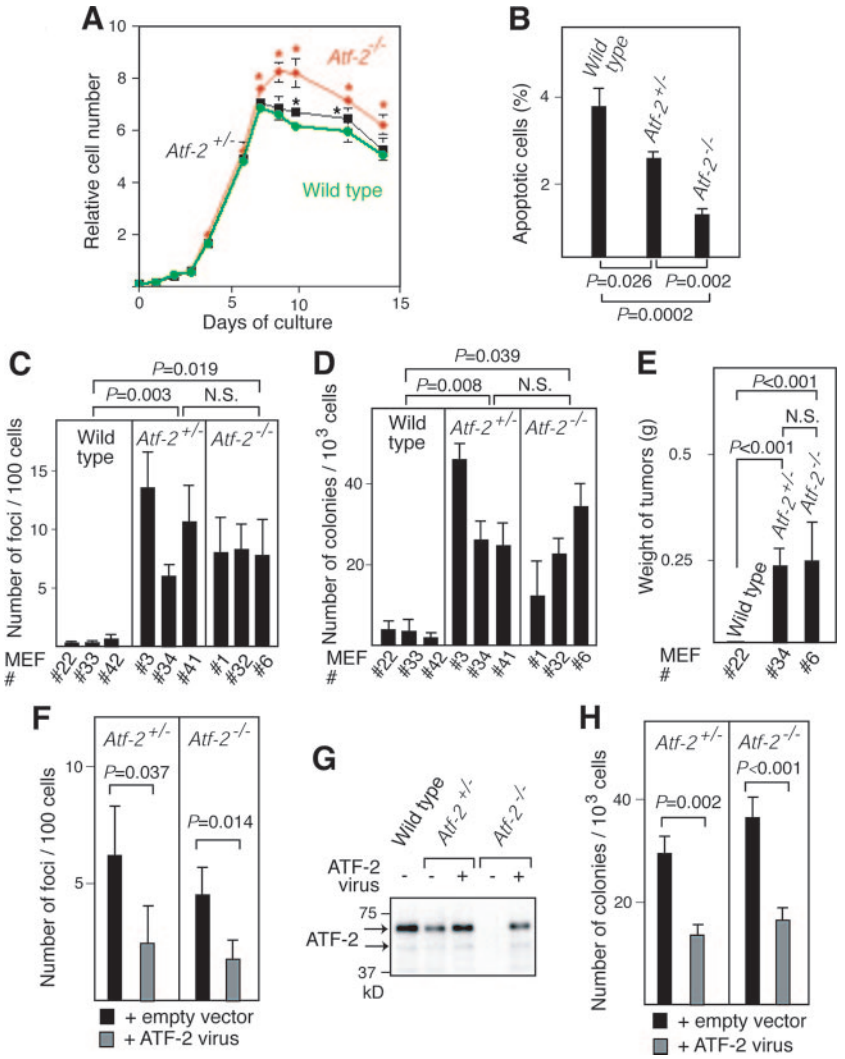

FIG. 3. The loss of one copy of *Atf-2* predisposes MEFs to tumorigenic transformation. (A) Growth curves of MEFs. The averages of three measurements with their SEM are shown. *, $P < 0.01$ compared to wild-type cells. (B) Decreased apoptosis in *Atf-2*$^{+/-}$ and *Atf-2*$^{-/-}$ cells at saturated cell density. Apoptotic cells at saturated cell density were detected by TUNEL labeling, and the percentages of apoptotic cells (mean plus SEM; $n = 3$) are shown. The *P* values obtained by Fisher's PLSD test are indicated (B to F and H). (C) The number of foci appearing after low-density seeding. The three independent MEFs used are indicated below each bar graph (C and D). The number of foci formed per 10^2 cells (mean plus SEM; $n = 3$) is indicated. N.S., no significant difference. (D) The number of colonies generated in methylcellulose after infection with v-K-*ras* virus. The number of colonies formed per 10^3 cells (mean plus SEM; $n = 3$) is indicated. (E) Weights of tumors formed 10 days after injection of the indicated MEFs generated in panel D into nude mice (12 sites of six mice). The average weights and SEM of the resulting 12 tumors from *Atf-2*$^{+/-}$ and *Atf-2*$^{-/-}$ cells are shown. No tumors were generated from wild-type cells. (F) Effects of reexpression of ATF-2 on the focus-forming capacities of *Atf-2* mutant cells. *Atf-2*$^{+/-}$ and *Atf-2*$^{-/-}$ MEFs were infected with the ATF-2-expressing virus and seeded, and the number of foci was measured as described in the legend to panel C. (G) Reexpression of ATF-2 in *Atf-2*$^{+/-}$ and *Atf-2*$^{-/-}$ cells. *Atf-2*$^{+/-}$ and *Atf-2*$^{-/-}$ cells expressing v-K-*ras* were infected with the virus encoding ATF-2 and the puromycin resistance marker, and the puromycin-resistant cell pools were selected. Whole-cell lysates were prepared and used for Western blotting with anti-ATF-2 antibody. (H) Effects of reexpression of ATF-2 on the colony-forming capacities of *Atf-2* mutant cells. Cells isolated in panel G were used for colony formation assays in methylcellulose, and the number of colonies was measured as described in the legend to panel D.

v-K-*ras*. Overexpression of *Gadd45*α partially but significantly suppressed the size of tumors generated by v-K-*ras*-expressing *Atf-2*$^{-/-}$ MEFs (Fig. 4G). Thus, both *Maspin* and *Gadd45*α suppressed the tumorigenicity of *Atf-2*$^{-/-}$ MEFs, indicating that down-regulation of these two genes contributes at least partly to transformation by a loss of *Atf-2*.

The c-Jun/ATF-2 heterodimers are more potent transcriptional activators than ATF-2 homodimers and regulate various genes that are implicated in growth control (3, 16, 50). In *Atf-2*$^{-/-}$ *p53*$^{-/-}$ and *p53*$^{-/-}$ MEFs, the levels of c-Jun alone, as well as the levels of CAT expression from the promoter containing the TRE, which may be mediated by endogenous c-Jun, were similar in both types of cells (Fig. 4H and I). Further, ectopically expressed c-Jun also similarly enhanced the CAT expression from the TRE-containing promoter in these cells. These results suggest that c-Jun function is not affected by a loss of *Atf-2* and that the tumorigenicity of *Atf-2*$^{-/-}$ MEFs is not due to the changes in c-Jun activity.

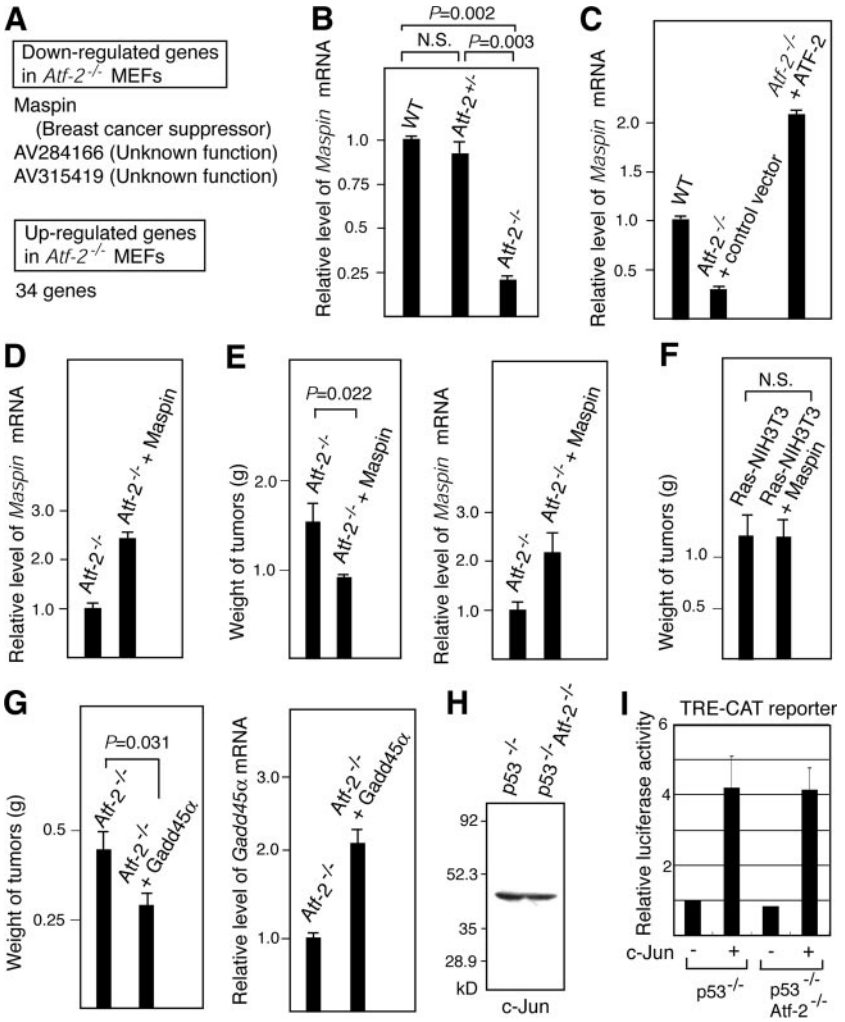

FIG. 4. A down-regulation of *Maspin* is correlated with the tumorigenicity of *Atf-2*$^{-/-}$ cells. (A) Identification of *Maspin* as an ATF-2 target gene in the absence of hypoxic stress. RNAs prepared from normally cultured *Atf-2*$^{-/-}$ and wild-type MEFs were subjected to DNA array analysis. Three and 34 genes were down- and up-regulated more than threefold by the loss of *Atf-2*, respectively. (B) Decreased levels of *Maspin* mRNA in *Atf-2*$^{-/-}$ cells. The *Maspin* mRNA levels in the indicated MEFs were analyzed by real-time RT-PCR, and the relative degree (mean plus SEM; $n = 3$) is indicated. (C) Ectopic expression of ATF-2 leads to up-regulation of *Maspin* expression. *Atf-2*$^{-/-}$ cells were infected with the retrovirus encoding ATF-2 and the puromycin resistance marker or control empty virus, and the puromycin-resistant cells were selected. *Maspin* mRNA levels were determined by real-time RT-PCR. (D) Reexpression of *Maspin* in *Atf-2*$^{-/-}$ cells. Cells were infected with the retrovirus encoding Maspin and the puromycin resistance marker, and the puromycin-resistant cells were selected. *Maspin* mRNA levels were determined by real-time RT-PCR. (E) *Maspin* overexpression suppresses the tumorigenicity of *Atf-2*$^{-/-}$ MEFs. *Atf-2*$^{-/-}$ MEFs expressing v-K-*ras* were infected with the *Maspin*-expressing virus or control empty virus and injected into 12 sites of six nude mice. The average weights and SEM of the 12 tumors that formed 14 days after the injection are shown (left). Note that double the number of cells were injected in these experiments as in Fig. 3E. *Maspin* mRNA levels in the tumors were determined by real-time RT-PCR (right). (F) *Maspin* does not suppress Ras-induced tumor formation. NIH 3T3 cells expressing activated K-*ras* were infected with the *Maspin*-expressing virus or control virus. Cells were injected into nude mice, and the weights of tumors formed were analyzed as described above. (G) *Gadd45*α overexpression suppresses the tumorigenicity of *Atf-2*$^{-/-}$ MEFs. *Atf-2*$^{-/-}$ MEFs expressing v-K-*ras* were infected with the *Gadd45*α-expressing virus or control empty virus and injected into nude mice. The weights of tumors formed were analyzed as described above (left). *Gadd45*α mRNA levels in the tumors were determined by real-time RT-PCR (right). (H) Loss of *Atf-2* does not affect c-Jun levels. Whole-cell lysates were prepared from *p53*$^{-/-}$ and *p53*$^{-/-}$ *Atf-2*$^{-/-}$ cells and used for Western blotting with anti-c-Jun antibody. (I) Loss of *Atf-2* does not affect c-Jun-dependent *trans*-activation. The CAT reporter, in which the TRE-containing promoter was linked to the CAT gene, was cotransfected into *p53*$^{-/-}$ and *p53*$^{-/-}$ *Atf-2*$^{-/-}$ cells with or without a c-Jun expression vector. CAT activity was measured, and the average of relative CAT activity ($n = 3$) is shown with SEM.

Mammary tumors in *Atf-2* heterozygous mice. The fact that *Atf-2*$^{+/-}$ MEFs exhibited a decrease in apoptosis and impaired *Gadd45*α induction compared to wild-type cells suggested that *Atf-2*$^{+/-}$ mice could be prone to tumor formation. Indeed, we found that, after a long latency period of about 60 weeks, female *Atf-2*$^{+/-}$ mice developed mammary tumors (Fig. 5A). These tumors occurred in 15 of 24 female *Atf-2*$^{+/-}$ mice, whereas all 20 age-matched, wild-type mice remained tumor free. *Atf-2*$^{+/-}$ male mice did not develop any tumors during a period of 105 weeks. The median time (T_{50}) for tumor-free survival of *Atf-2*$^{+/-}$ female mice was about 90 weeks. Histological analyses indicated that these tumors included invasive

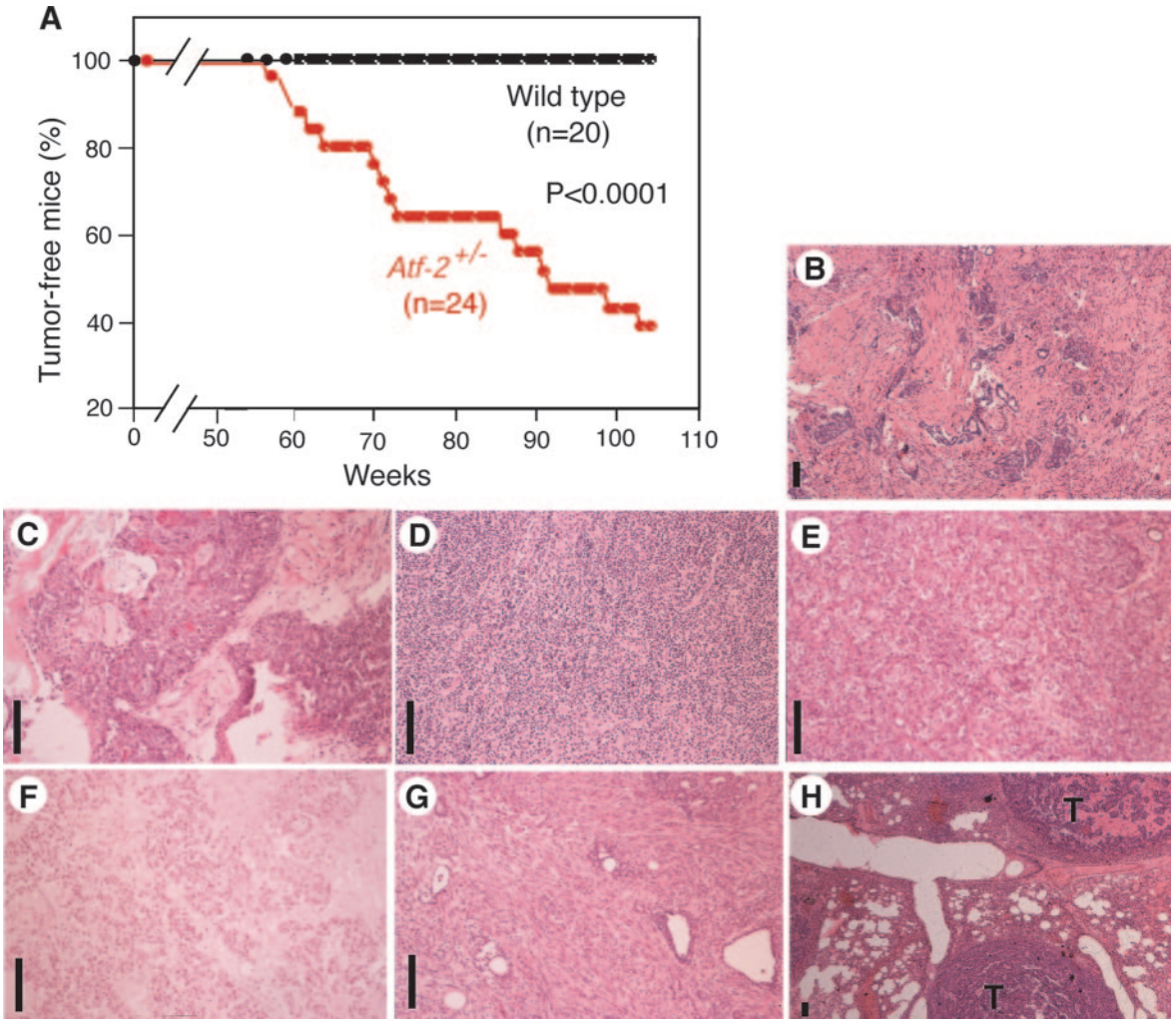

FIG. 5. Female *Atf-2*$^{+/-}$ mice spontaneously develop mammary tumors. (A) Kaplan-Meier tumor-free survival curves of *Atf-2*$^{+/-}$ and wild-type mice. The *P* value obtained by Fisher's PLSD test is also shown. The mammary tumors of 15/24 *Atf-2*$^{+/-}$ mice are described in Table 1. (B to H) Histology of the mammary tumors of *Atf-2*$^{+/-}$ mice, showing invasive ductal carcinomas with scirrhous (B), squamous (C), anaplastic (D), solid-tubular (E), and papillary (F) invasion; a sarcomatoid carcinoma with spindle cell invasion (G); and a carcinoma that had metastasized to the lung (H). Bar, 100 μm. T, tumor.

ductal carcinomas with scirrhous, squamous, anaplastic, solid-tubular, and papillary invasion and a sarcomatoid carcinoma with spindle cell invasion (Fig. 5B to G and Table 1). In one case (tumor T2), metastasis of a carcinoma to the lung was also observed (Fig. 5H). Invasive ductal carcinoma with scirrhous invasion, which was most frequently found in *Atf-2*$^{+/-}$ mice, is also a common human breast cancer (37).

Most of the tumor suppressor genes identified to date fulfill Knudson's "two-mutation" criterion, in which tumors arise if both alleles have mutations or expression from both alleles is suppressed (23). DNA sequence analysis of the wild-type *Atf-2* allele in 11 mammary tumors revealed no mutations in the ATF-2 protein-coding region (data not shown). Results of an RT-PCR analysis indicated that of these 11 tumors, *Atf-2* mRNA was undetectable in five, significantly reduced in four, and not affected in two (Fig. 6A and Table 1). Western blotting using whole-cell lysates from mammary tumors indicated that the ATF-2 proteins were almost undetectable in all the tumors examined (Fig. 6B). These results suggest that ATF-2 is also regulated at the posttranscriptional level. Consistent with these observations, no ATF-2 immunostaining signals were observed in the tumors that did not express *Atf-2* mRNA, whereas ATF-2 was localized in the nuclei of normal mammary epithelial cells (Fig. 6E, F, and G). These results indicate that *Atf-2* heterozygosity predisposes mice to develop mammary tumors and that severe reduction of ATF-2 expression may enhance tumor development. Although the c-Jun level dramatically decreased in only 1 tumor, the significant levels of c-Jun were detected in 10 tumors (Fig. 6D). These results suggest that the c-Jun levels are not dramatically affected in most of the mammary tumors of *Atf-2*$^{+/-}$ mice. Aberrant DNA methylation of CpG islands around promoter regions can suppress transcription (1). However, the results of a methylation-specific PCR analysis using the bisulfite method did not reveal a significant increase in the degree of methylation of the *Atf-2* promoter region in mammary tumors (data not shown). Thus, the wild-

TABLE 1. Tumors in *Atf-2*$^{+/-}$ mice

Mouse	Sex[a]	Age (wk)	Site	Histology[b]	Expression[d]			
					Atf-2	*p53*	*Maspin*	*Gadd45*α
T2	F	57	Mammary gland	Idc. scirrhous	ND	ND	ND	ND
T1	F	70	Mammary gland	Idc. scirrhous	ND	ND	ND	ND
T8	F	72	Mammary gland	Idc. scirrhous	+	+	Red	Red
T5	F	73	Mammary gland	Idc. scirrhous	−	−	−	−
T7	F	91	Mammary gland	Idc. scirrhous	−	+	−	−
C21	F	86	Mammary gland	Idc. squamous	−	+	−	−
T4	F	88	Mammary gland	Idc. squamous	Red	+	−	−
C22	F	92	Mammary gland	Idc. squamous	Red	+	−	Red
104	F	60	Mammary gland	Idc. anaplastic	Red	+	−	−
T6	F	62	Mammary gland	Idc. solid-tubular	Red	+	Red	Red
T13	F	99	Mammary gland	Idc. Papillary	−	Red	−	−
105	F	64	Mammary gland	Sarc. ca. spindle cell	−	−	−	−
C25	F	59	Mammary gland	Unknown	+	+	Red	Red
T3	F	71	Mammary gland	ND[c]	ND	ND	ND	ND
T16	F	103	Mammary gland	ND	ND	ND	ND	ND

[a] F, female.
[b] Idc. scirrhous, invasive ductal carcinoma with scirrhous invasion; Idc. squamous, invasive ductal carcinoma with squamous invasion; Idc. anaplastic, invasive ductal carcinoma with anaplastic invasion; Idc. solid-tubular, invasive ductal carcinoma with solid-tubular invasion; Idc. papillary, invasive ductal carcinoma with papillary invasion; Sarc. ca. spindle cell, sarcomatoid carcinoma with spindle cell invasion.
[c] ND, not determined due to degradation of tumor tissues and mRNA.
[d] +, the expression level was almost the same as that in the wild-type mammary gland; −, almost no expression; Red, the expression level was reduced to 10% to 60% of that in the wild-type mammary gland.

type *Atf-2* allele in the mammary tumors may be silenced by unknown mechanisms, such as the mutation of positive regulators of *Atf-2* gene transcription.

Decreased levels of *Maspin* and *GADD45*α mRNA and chromosome instability in mammary tumors of *Atf-2*$^{+/-}$ mice. Since ATF-2 is involved in some types of apoptosis to which most cell types are probably susceptible, some of the ATF-2 target genes that we identified in MEFs could be shared by mammary epithelial cells. To test this notion, we analyzed the *Maspin* and *Gadd45*α expression in 11 mammary tumors from *Atf-2*$^{+/-}$ mice (Fig. 6A and Table 1). *Maspin* expression was lost in eight tumors and reduced in the remaining three, while *Gadd45*α expression was lost in seven tumors and reduced in four. In particular, in all five tumors that did not express detectable *Atf-2* mRNA, neither *Maspin* nor *Gadd45*α mRNA was detected. With regard to protein expression, Maspin proteins were undetectable in eight tumors and significantly reduced in two tumors (Fig. 6C). Furthermore, no GADD45α immunostaining signals were observed in the tumors that did not express *Atf-2* mRNA, whereas the wild-type mammary gland appeared to express GADD45α (Fig. 6H). *p53* mRNA expression was lost in two tumors and reduced in one tumor but was not reduced in the remaining eight tumors (Fig. 6A and Table 1). Neither the estrogen receptor nor c-ErbB-2, two well-known markers of certain types of breast cancers, was expressed in tumors from the *Atf-2*$^{+/-}$ mice (data not shown).

Breast cancer cells often exhibit genomic instability (51), which has also been observed in *Gadd45*α-deficient mice (15). We performed CGH to assess genomic changes in four independent breast tumors from *Atf-2*$^{+/-}$ mice. An overview of the changes that we detected is shown in Fig. 7A. All four tumors analyzed showed copy number aberrations, with gains predominating over losses at a ratio of 2.25:1. The numbers of aberrations per tumor were five (tumors C21 and 105), two (tumor C22), and one (tumor T6). High-level amplification, indicative of gene amplification, was detected only at chromosome 17q in tumor T6 (Fig. 7B). Thus, mammary tumors from *Atf-2*$^{+/-}$ mice exhibit genomic instability.

Decreased levels of *ATF-2* mRNA in human breast cancers. To investigate whether ATF-2 acts as a tumor susceptibility gene of human breast cancers, we determined the *ATF-2* mRNA levels in human breast cancer cells isolated by the laser capture microdissection technique, which allowed us to selectively isolate epithelial cells. The *ATF-2* expression levels in invasive ductal carcinomas with solid-tubular and scirrhous invasion and in ductal carcinoma in situ were about one-fifth to one-half of those found in normal breast epithelial cells (statistical analysis indicated a P value of 0.005) (Fig. 8A, left). On average, the *ATF-2* mRNA level in 10 breast cancers of various types was about half of that in normal mammary epithelial cells (Fig. 8A, middle). Furthermore, analysis of specific types of breast cancers indicated that the *ATF-2* mRNA levels in invasive ductal carcinomas with scirrhous, solid-tubular, and papillotubular invasion were 45%, 50%, and 60% lower, respectively, than the levels in normal mammary epithelial cells (Fig. 8A, right). Statistical analysis of these results indicated that the decreased levels of *ATF-2* mRNA in human breast cancers were significant ($P < 0.01$). These findings suggest that *ATF-2* may act as a tumor susceptibility gene for various types of breast cancers in humans.

A decrease in ATF-2 correlates with tumorigenicity of HMEC. We next examined the tumorigenic effect of knocking down ATF-2 levels in the normal HMEC-derived cell line MCF12A by using RNA interference. MCF12A cells express levels of *ATF-2* mRNA similar to those of HMEC (Fig. 8B). The ATF-2 double-stranded RNA expression plasmid was constructed using the pDECAP vector, which we recently developed (43), and introduced into MCF12A cells to generate MCF12A-ATF2-RNAi cells. In these cells, *ATF-2* mRNA levels were about one-fourth of the level in control MCF12A cells

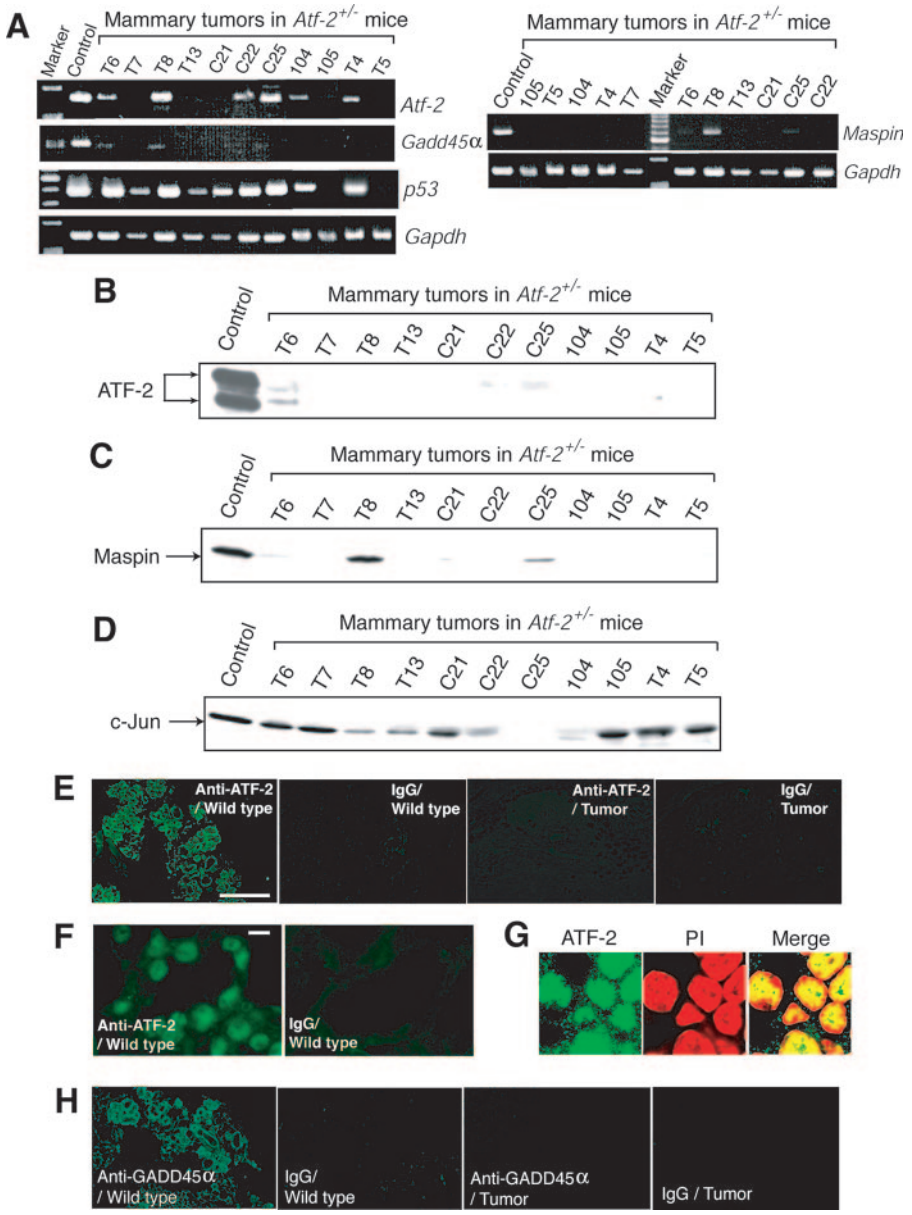

FIG. 6. Down-regulation of *Atf-2*, *Gadd45*α, and *Maspin* in mammary tumors of *Atf-2*$^{+/-}$ mice. (A) RT-PCR analysis of *Atf-2*, *Gadd45*α, *Maspin*, *p53*, and *Gapdh* mRNAs in mammary tumors of *Atf-2*$^{+/-}$ mice. In the control lane, RNA from normal mammary tissue of *Atf-2*$^{+/-}$ mice served as the template. (B, C, and D) Levels of ATF-2, Maspin, and c-Jun proteins. Whole-cell lysates were prepared from mammary tumors of *Atf-2*$^{+/-}$ mice and used for Western blotting with anti-ATF-2 (B), anti-Maspin (C), or anti-c-Jun (D) antibodies. (E to H) Immunostaining of ATF-2 and Gadd45α. Sections of normal mammary gland or the T7 mammary tumors from *Atf-2*$^{+/-}$ mice (Table 1) were stained with anti-ATF-2 (E, F, and G) or anti-Gadd45α (H) antibody or control IgG. Lower (E) and higher (F) magnifications are indicated. Bars: D, 500 μm; E, 10 μm. In panel G, the nuclear localization of ATF-2 is indicated by costaining with propidium iodide (PI).

harboring the empty vector (Fig. 8B). We found that when MCF12A and MCF12A-ATF2-RNAi cells were infected with a v-K-*ras* retrovirus and injected into nude mice, MCF12A-ATF2-RNAi cells were significantly more tumorigenic than MCF12A cells (Fig. 8C).

We also examined the *ATF-2* mRNA levels of several cell lines established from human breast cancers and found that the SK-BR3 cell line expressed lower levels of *ATF-2* mRNA than the others (Fig. 8D). To assess the effect of elevating ATF-2 expression in SK-BR3 cells, they were transfected with the ATF-2 expression vector. These transfectants expressed 60% higher levels of *ATF-2* mRNA (Fig. 8D) and reached 25% lower cell densities than the control SK-BR3 cells harboring the empty vector (Fig. 8E). In addition, the population of apoptotic cells at saturated cell density was also increased from 1.5% to 3.4% by overexpression of ATF-2 (Fig. 8F). After infection with a v-K-*ras* retrovirus, SK-BR3 cells overexpressing ATF-2 did not produce either visible foci after low-density seeding or colonies in soft agarose, unlike the control SK-BR3 cells (Fig. 8G and H).

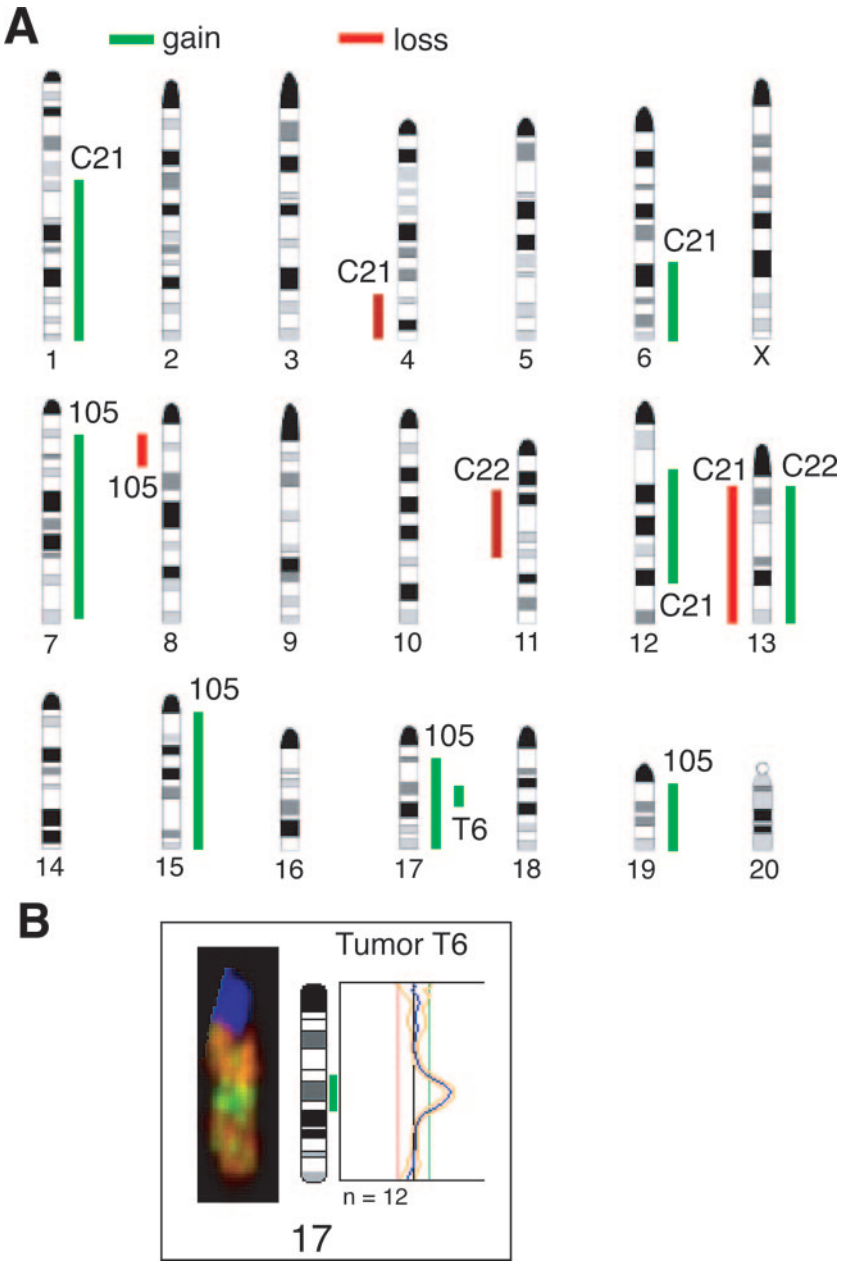

FIG. 7. The mammary tumors of *Atf-2*$^{+/-}$ mice exhibit chromosome instability. (A) Summary of the CGH-detected genomic imbalances in 29 esophageal squamous cell carcinoma cell lines using four mammary tumors (C22, C21, T6, and 105, described in Table 1). The vertical lines on the left of each chromosome show losses of genomic material in cell lines, whereas those on the right correspond to copy number gains. (B) High-level gain indicative of gene amplification was detected in tumor T6 at chromosome 17q. Representative CGH images of chromosome 17 (left) and its profile (right) are shown.

DISCUSSION

The present study indicates that a decrease in ATF-2 expression leads to development of breast cancers. This is correlated with higher cell density in *Atf-2*$^{-/-}$ MEFs, which may be related to a decrease in *Maspin* expression, resulting in decreased apoptosis at saturated cell density. Perturbation in p38 signaling is known to increase susceptibility to mammary tumors by a variety of downstream pathways (5, 22, 34), and our results are consistent with these previous studies. It is known that *Gadd45*α, an ATF-2 target, contributes to p38 activation (30). Thus, there is another potential positive feedback loop involving p38, ATF-2, and Gadd45α whose disturbance can be tumorigenic in breast epithelial cells. Although we have focused on the two ATF-2 target genes, *Gadd45*α and *Mapin*, in the present study, it is unlikely that the down-regulation of only these two genes leads to mammary tumors. We have identified 39 genes which are regulated by ATF-2 in response to hypoxia, and probably the changed expression of multiple ATF-2 target genes, including these, cooperatively contributes to the generation of mammary tumors in *Atf-2*$^{+/-}$

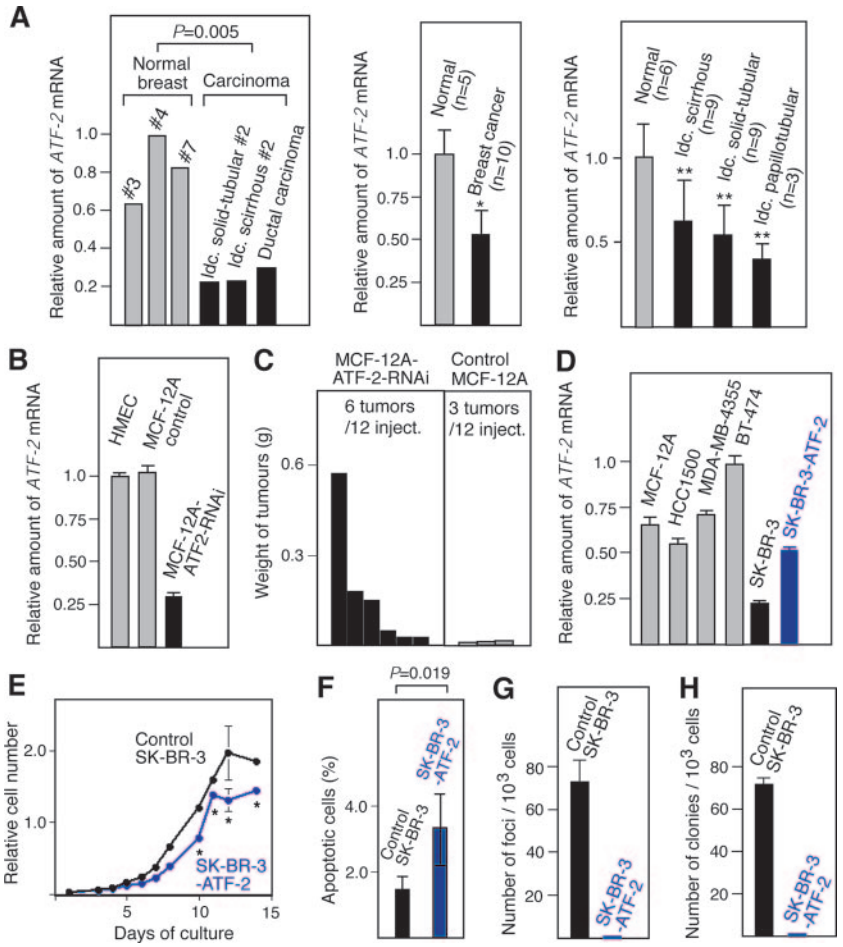

FIG. 8. *ATF-2* expression in human breast cancer tissues and role of ATF-2 in the growth regulation of HMEC. (A) *ATF-2* mRNA levels in human breast cancer cells and normal mammary epithelial cells isolated by the laser capture microdissection technique. It was confirmed that there were comparable levels of epithelial cells in both samples. The *ATF-2* mRNA levels were measured by quantitative real-time RT-PCR using RNAs prepared from individual breast cancers (left), 10 breast cancers of various types (middle) (*, $P = 0.01$), specific types of breast cancers (right) (**, $P < 0.01$), or normal mammary glands. (B) RNA interference decreases the *ATF-2* mRNA levels in HMEC. *ATF-2* mRNA levels in HMEC, control MCF12A cells harboring empty vector, and MCF12A cells expressing *ATF-2* double-stranded RNA (MCF12A-ATF2-RNAi) were measured by real-time RT-PCR. (C) Decreased *ATF-2* expression elevates the susceptibility of HMEC to tumorigenesis. MCF12A and MCF12A-ATF2-RNAi cells were infected with the v-K-*ras*-bearing retrovirus and injected into 12 sites of six nude mice. The tumors and their weights are indicated. (D) *ATF-2* mRNA levels in several human breast cancer cell lines and SK-BR3 cells transformed with an ATF-2-expressing vector were measured by real-time RT-PCR. (E to G) Effects of ATF-2 overexpression on the growth of SK-BR3 cells. Growth curves of ATF-2-overexpressing SK-BR3 cells and control SK-BR3 cells harboring the empty vector are shown (E) (*, $P < 0.04$). Apoptotic cells at saturated cell density were counted, and the percentages of apoptotic cells (mean plus SEM; $n = 3$) are shown (F). The number of foci appearing after low-density seeding (G) and the number of colonies that formed in soft agarose after infection with v-K-*ras* retrovirus (H) are also indicated. The averages of triplicate measurements and their SEM are shown.

mice. Although the ectopic expression of *Maspin* or *Gadd45*α partially suppressed the tumorigenicity of Ras-expressing *Atf-2*$^{-/-}$ MEFs (Fig. 4E and G), the ectopic expression of *Maspin* or *Gadd45*α alone may not be enough to suppress the tumorigenicity of v-K-*ras*-expressing *Atf-2*$^{-/-}$ MEFs. Since defects in hypoxia-induced apoptosis have not been reported in *Gadd45*α mutant mice (15), multiple genes may be involved in the hypoxia-induced apoptosis. Therefore, the ectopic expression of multiple ATF-2 target genes in addition to *Gadd45*α may be necessary to rescue the defects in the hypoxia-induced apoptosis of *Atf-2*$^{-/-}$ cells.

The 978 genes were down-regulated by a loss of ATF-2 in the presence of hypoxic stress, while only 3 genes, including *Maspin*, were down-regulated in the absence of hypoxic stress. This big difference in the number of target genes may be explained by multiple mechanisms. The *p53*$^{-/-}$ cells were used to identify 978 genes, whereas *p53*$^{+/+}$ cells were used to identify 3 genes. Induction of some hypoxia-induced ATF-2 target genes might be detected in *p53*$^{-/-}$ cells but not in *p53*$^{+/+}$ cells. For instance, hypoxic stress induces a group of the repair-related genes via activation of ATM, which directly phosphorylates ATF-2 (4). Induction of these genes may not be detected in *p53*$^{+/+}$ cells, because apoptosis and cessation of the cell cycle mediated by p53 occur in response to hypoxic stress in *p53*$^{+/+}$ cells. Alternatively, some of the 978 genes might be synergistically up-regulated by both ATF-2 and other transcription factors that are activated or induced by hypoxic stress. Hypoxia induces the expression of many genes, including tran-

scription factors, and also activates some transcription factors, such as the HIF family of proteins (20).

Notably, while ATF-2 is ubiquitously expressed in all cell types (45), *Atf-2*$^{+/-}$ mice developed only mammary tumors. This suggests that there may be some mammary epithelial cell-specific target genes of ATF-2 that are critical for mammary-tumor development. While the identification of these target genes is a subject for future investigation, down-regulation of *Maspin* and *Gadd45*α in mammary tumors of *Atf-2*$^{+/-}$ mice suggests that these two genes may contribute, at least partly, to the development of mammary tumors. *Maspin* was recently shown to enhance cellular sensitivity to apoptotic stimuli (25). Thus, decreased *Maspin* expression could contribute, at least partly, to immortalization by abrogating the apoptosis induced by cell-cell interactions or various signals. Once immortalized, *Atf-2*$^{+/-}$ and *Atf-2*$^{-/-}$ cells have a lower capacity than wild-type cells to induce apoptosis in response to hypoxia via the down-regulation of a group of genes that includes *GADD45*α. It is believed that solid tumors, such as mammary tumors, are exposed to hypoxic stress. *GADD45*α is involved in the control of apoptosis and cell cycle arrest at G_2/M, as well as in DNA damage repair and genomic stability. Similar to what occurs in *Gadd45*α-deficient cells (15), we also observed chromosome instability in mammary tumors from *Atf-2*$^{+/-}$ mice. It is known that a hypoxic microenvironment of solid tumors correlates with their increased malignancy and potential for metastasis (14). Therefore, the lower susceptibility of *Atf-2*-deficient cells to hypoxia-induced apoptosis may promote the development of a malignant phenotype.

Various types of mammary tumors developed in *Atf-2*$^{+/-}$ mice, including invasive ductal carcinomas with scirrhous and squamous invasion, common types of human breast cancers. Consistent with this, a decrease in the *ATF-2* mRNA levels was also observed in various types of human breast cancers, including invasive ductal carcinomas with scirrhous, solid-tubular, and papillotubular invasion. We tried to examine the relationship between a decrease in the *ATF-2* mRNA in human breast cancers and the change in expression levels of the putative target genes using expression-profiling data from human breast cancer patients. However, we could not obtain a clear answer, because the level of *ATF-2* mRNA in the healthy human breast is too low to be accurately measured by using the DNA array method, although it can be precisely measured by using the real-time RT-PCR method. Identification of the *ATF-2* gene as a breast cancer susceptibility gene may be useful for individualized breast cancer risk assessment and could potentially lead to a reduction in breast cancer incidence. Since it is likely that hypoxia and defective apoptosis lead to genomic instability and the development of solid tumors, ATF-2 may contribute not only to breast cancers, but also to other types of cancers in humans.

ACKNOWLEDGMENTS

We are grateful to H. Kanda for histological analysis, K. Fukumoto for DNA array analysis, M. Noda for murine leukemia virus, H. Saito for the GADD45α plasmid, K. Fukumoto for DNA array analysis, and members of the Experimental Animal Division of RIKEN Tsukuba Institute for maintenance of the mice.

This work was supported in part by Grants-in-Aid for Scientific Research and by grants from the Genome Network Project of the Ministry of Education, Culture, Sports, Science and Technology of Japan.

REFERENCES

1. **Baylin, S., and T. H. Bestor.** 2002. Altered methylation patterns in cancer cell genomes: cause or consequence? Cancer Cell **1:**299–305.
2. **Beier, F., R. J. Lee, A. C. Taylor, R. G. Pestell, and P. LuValle.** 1999. Identification of the cyclin D1 gene as a target of activating transcription factor 2 in chondrocytes. Proc. Natl. Acad. Sci. USA **96:**1433–1438.
3. **Benbrook, D. M., and N. C. Jones.** 1990. Heterodimer formation between CREB and JUN proteins. Oncogene **5:**295–302.
4. **Bhoumik, A., S. Takahashi, W. Breitweiser, Y. Shiloh, N. Jones, and Z. Ronai.** 2005. ATM-dependent phosphorylation of ATF2 is required for the DNA damage response. Mol. Cell **18:**577–587.
5. **Bulavin, D. V., C. Phillips, B. Nannenga, O. Timofeev, L. A. Donehower, C. W. Anderson, E. Appella, and A. J. Fornace, Jr.** 2004. Inactivation of the Wip1 phosphatase inhibits mammary tumorigenesis through p38 MAPK-mediated activation of the $p16^{Ink4a}$-$p19^{Arf}$ pathway. Nat. Genet. **36:**343–350.
6. **Chang, L., and M. Karin.** 2001. Mammalian MAP kinase signalling cascades. Nature **410:**37–40.
7. **Dignam, J. D., R. M. Lebovitz, and R. G. Roeder.** 1983. Accurate transcription initiation by RNA polymerase II in a soluble extract from isolated mammalian nuclei. Nucleic Acids Res. **11:**1475–1489.
8. **Falvo, J. V., B. S. Parekh, C. H. Lin, E. Fraenkel, and T. Maniatis.** 2000. Assembly of a functional beta-interferon enhanceosome is dependent on ATF-2-c-jun heterodimer orientation. Mol. Cell. Biol. **20:**4814–4825.
9. **Fukuda, Y., N. Kurihara, I. Imoto, K. Yasui, M. Yoshida, K. Yanagihara, J. G. Park, Y. Nakamura, and J. Inazawa.** 2000. CD44 is a potential target of amplification within the 11p13 amplicon detected in four of 25 gastric cancer cell lines. Genes Chromosome Cancer **29:**315–324.
10. **Gaire, M., B. Chatton, and C. Kedinger.** 1990. Isolation and characterization of two novel, closely related ATF cDNA clones from HeLa cells. Nucleic Acids Res. **18:**3467–3473.
11. **Gupta, S., D. Campbell, B. Dérijard, and R. J. Davis.** 1995. Transcription factor ATF2 regulation by the JNK signal transduction pathway. Science **267:**389–393.
12. **Hai, T., and T. Curran.** 1991. Cross-family dimerization of transcription factors Fos/Jun and ATF/CREB alters DNA binding specificity. Proc. Natl. Acad. Sci. USA **88:**3720–3724.
13. **Hai, T. W., F. Liu, E. A. Allegretto, M. Karin, and M. R. Green.** 1988. A family of immunologically related transcription factors that includes multiple forms of ATF and AP-1. Genes Dev. **2:**1216–1226.
14. **Hockel, M., and P. Vaupel.** 2001. Tumor hypoxia: definitions and current clinical, biologic, and molecular aspects. J. Natl. Cancer Inst. **93:**266–276.
15. **Hollander, M. C., M. S. Sheikh, D. V. Bulavin, K. Lundgren, L. Augeri-Henmueller, R. Shehee, T. A. Molinaro, K. E. Kim, E. Tolosa, J. D. Ashwell, M. P. Rosenberg, Q. Zhan, P. M. Fernandez-Salguero, W. F. Morgan, C. X. Deng, and A. J. Fornace, Jr.** 1999. Genomic instability in *Gadd45*α-deficient mice. Nat. Genet. **23:**176–184.
16. **Huguier, S., J. Baguet, S. Perez, H. van Dam, and M. Castellazzi.** 1998. Transcription factor ATF2 cooperates with v-Jun to promote growth factor-independent proliferation in vitro and tumor formation in vivo. Mol. Cell. Biol. **18:**7020–7029.
17. **Ivashkiv, L. B., H. C. Liou, C. J. Kara, W. W. Lamph, I. M. Verma, and L. H. Glimcher.** 1990. mXBP/CRE-BP2 and c-Jun form a complex which binds to the cyclic AMP, but not to the 12-O-tetradecanoylphorbol-13-acetate, response element. Mol. Cell. Biol. **10:**1609–1621.
18. **Jin, W., T. Takagi, S. N. Kanesashi, T. Kurahashi, T. Nomura, J. Harada, and S. Ishii.** 2006. Schnurri-2 controls BMP-dependent adipogenesis via interaction with Smad proteins. Dev. Cell. **10:**461–471.
19. **Kaelin, W. G.** 2005. Proline hydroxylation and gene expression. Annu. Rev. Biochem. **74:**115–128.
20. **Kamijo, T., F. Zindy, M. F. Roussel, D. E. Quelle, J. R. Downing, R. A. Ashmun, G. Grosveld, and C. J. Sherr.** 1997. Tumor suppression at the mouse INK4a locus mediated by the alternative reading frame product p19ARF. Cell **91:**649–659.
21. **Kastan, M. B., Q. Zhan, W. S. el-Deiry, F. Carrier, T. Jacks, W. V. Walsh, B. S. Plunkett, B. Vogelstein, and A. J. Fornace, Jr.** 1992. A mammalian cell cycle checkpoint pathway utilizing p53 and GADD45 is defective in ataxia-telangiectasia. Cell **71:**587–597.
22. **Kim, M. S., E. J. Lee, H. R. Kim, and A. Moon.** 2003. p38 kinase is a key signaling molecule for H-Ras-induced cell motility and invasive phenotype in human breast epithelial cells. Cancer Res. **63:**5454–5461.
23. **Knudson A. G., Jr.** 1971. Mutation and cancer: statistical study of retinoblastoma. Proc. Natl. Acad. Sci. USA **68:**820–823.
24. **Kondo, S., T. Murakami, K. Tatsumi, M. Ogata, S. Kanemoto, K. Otori, K. Iseki, A. Wanaka, and K. Imaizumi.** 2005. OASIS, a CREB/ATF-family member, modulates UPR signalling in astrocytes. Nat. Cell Biol. **7:**186–194.
25. **Liu, J., S. Yin, N. Reddy, C. Spencer, and S. Sheng.** 2004. Bax mediates the apoptosis-sensitizing effect of maspin. Cancer Res. **64:**1703–1711.
26. **Livingstone, C., G. Patel, and N. Jones.** 1997. ATF-2 contains a phosphorylation-dependent transcriptional activation domain. EMBO J. **14:**1785–1797.

27. **Maekawa, T., F. Bernier, M. Sato, S. Nomura, M. Singh, Y. Inoue, T. Tokunaga, H. Imai, M. Yokoyama, A. Reimold, L. H. Glimcher, and S. Ishii.** 1999. Mouse ATF-2 null mutants display features of a severe type of meconium aspiration syndrome. J. Biol. Chem. **274:**17813–17819.
28. **Maekawa, T., H. Sakura, C. Kanei-Ishii, T. Sudo, T. Yoshimura, J. Fujisawa, M. Yoshida, and S. Ishii.** 1989. Leucine zipper structure of the protein CRE-BP1 binding to the cyclic AMP response element in brain. EMBO J. **8:**2023–2028.
29. **Matsuda, S., T. Maekawa, and S. Ishii.** 1991. Identification of the functional domains of the transcriptional regulator CRE-BP1. J. Biol. Chem. **266:**18188–18193.
30. **Mita, H., J. Tsutsui, M. Takekawa, E. A. Witten, and H. Saito.** 2002. Regulation of MTK1/MEKK4 kinase activity by its N-terminal autoinhibitory domain and GADD45 binding. Mol. Cell. Biol. **22:**4544–4555.
31. **Morooka, H., J. V. Bonventre, C. M. Pombo, J. M. Kyriakis, and T. Force.** 1995. Ischemia and reperfusion enhance ATF-2 and c-Jun binding to cAMP response elements and to an AP-1 binding site from the c-*jun* promoter. J. Biol. Chem. **270:**30084–30092.
32. **Morrison, D. K., and R. J. Davis.** 2003. Regulation of MAP kinase signaling modules by scaffold proteins in mammals. Annu. Rev. Cell Dev. Biol. **19:**91–118.
33. **Nagadoi, A., K. Nakazawa, H. Uda, K. Okuno, T. Maekawa, S. Ishii, and Y. Nishimura.** 1999. Solution structure of the transactivation domain of ATF-2 comprising a zinc finger-like subdomain and a flexible subdomain. J. Mol. Biol. **287:**593–607.
34. **Neve, R. M., T. Holbro, and N. E. Hynes.** 2002. Distinct roles for phosphoinositide 3-kinase, mitogen-activated protein kinase and p38 MAPK in mediating cell cycle progression of breast cancer cells. Oncogene **21:**4567–4576.
35. **Nomura, N., Y. L. Zu, T. Maekawa, S. Tabata, T. Akiyama, and S. Ishii.** 1993. Isolation and characterization of a novel member of the gene family encoding the cAMP response element-binding protein CRE-BP1. J. Biol. Chem. **268:**4259–4266.
36. **Ouwens, D. M., N. D. de Ruiter, G. C. van der Zon, A. P. Carter, J. Schouten, C. van der Burgt, K. Kooistra, J. L. Bos, J. A. Maassen, and H. van Dam.** 2002. Growth factors can activate ATF2 via a two-step mechanism: phosphorylation of Thr71 through the Ras-MEK-ERK pathway and of Thr69 through RalGDS-Src-p38. EMBO J. **21:**3782–3793.
37. **Page, D. L., and T. J. Anderson.** 1987. Diagnostic histopathology of the breast. Churchill Livingstone, London, United Kingdom.
38. **Persengiev, S. P., and M. R. Green.** 2003. The role of ATF/CREB family members in cell growth, survival and apoptosis. Apoptosis **8:**225–228.
39. **Reimold, A. M., M. J. Grusby, B. Kosaras, J. W. Fries, R. Mori, S. Maniwa, I. M. Clauss, T. Collins, R. L. Sidman, M. J. Glimcher, and L. H. Glimcher.** 1996. Chondrodysplasia and neurological abnormalities in ATF-2-deficient mice. Nature **379:**262–265.
40. **Sano, Y., J. Harada, S. Tashiro, R. Gotoh-Mandeville, T. Maekawa, and S. Ishii.** 1999. ATF-2 is a common nuclear target of Smad and TAK1 pathways in transforming growth factor-β signaling. J. Biol. Chem. **274:**8949–8957.
41. **Sano, Y., F. Tokitou, P. Dai, T. Maekawa, T. Yamamoto, and S. Ishii.** 1998. CBP alleviates the intramolecular inhibition of ATF-2 function. J. Biol. Chem. **273:**29098–29105.
42. **Shimizu, M., Y. Nomura, H. Suzuki, E. Ichikawa, A. Takeuchi, M. Suzuki, T. Nakamura, T. Nakajima, and K. Oda.** 1998. Activation of the rat cyclin A promoter by ATF2 and Jun family members and its suppression by ATF4. Exp. Cell Res. **239:**93–103.
43. **Shinagawa, T., and S. Ishii.** 2003. Generation of *Ski*-knockdown mice by expressing a long double-strand RNA from an RNA polymerase II promoter. Genes Dev. **17:**1340–1345.
44. **Shinagawa, T., T. Nomura, C. Colmenares, M. Ohira, A. Nakagawara, and S. Ishii.** 2001. Increased susceptibility to tumorigenesis of *ski*-deficient heterozygous mice. Oncogene **20:**8100–8108.
45. **Takeda, J., T. Maekawa, T. Sudo, Y. Seino, H. Imura, N. Saito, C. Tanaka, and S. Ishii.** 1991. Expression of the CRE-BP1 transcriptional regulator binding to the cyclic AMP response element in central nervous system, regenerating liver, and human tumors. Oncogene **6:**1009–1114.
46. **Takekawa, M., and H. Saito.** 1998. A family of stress-inducible GADD45-like proteins mediate activation of the stress-responsive MTK1/MEKK4 MAPKKK. Cell **95:**521–530.
47. **Tamura, K., B. Hua, S. Adachi, I. Guney, J. Kawauchi, M. Morioka, M. Tamamori-Adachi, Y. Tanaka, Y. Nakabeppu, M. Sunamori, J. M. Sedivy, and S. Kitajima.** 2005. Stress response gene *ATF3* is a target of c-myc in serum-induced cell proliferation. EMBO J. **24:**2590–2601.
48. **van Dam, H., M. Duyndam, R. Rottier, A. Bosch, L. de Vries-Smits, P. Herrlich, A. Zantema, P. Angel, and A. J. van der Eb.** 1993. Heterodimer formation of cJun and ATF-2 is responsible for induction of c-*jun* by the 243 amino acid adenovirus E1A protein. EMBO J. **12:**479–487.
49. **van Dam, H., D. Wilhelm, I. Herr, A. Steffen, P. Herrlich, and P. Angel.** 1997. ATF-2 is preferentially activated by stress-activated protein kinases to mediate c-*jun* induction in response to genotoxic agents. EMBO J. **14:**31798–31811.
50. **van Dam, H., S. Huguier, K. Kooistra, J. Baguet, E. Vial, A. J. van der Eb, P. Herrlich, P. Angel, and M. Castellazzi.** 1998. Autocrine growth and anchorage independence: two complementing Jun-controlled genetic programs of cellular transformation. Genes Dev. **12:**1227–1239.
51. **Venkitaraman, A. R.** 2002. Cancer susceptibility and the functions of BRCA1 and BRCA2. Cell **108:**171–182.
52. **Yasui, K., I. Imoto, Y. Fukuda, A. Pimkhaokham, Z. Q. Yang, T. Naruto, Y. Shimada, Y. Nakamura, and J. Inazawa.** 2001. Identification of target genes within an amplicon at 14q12-q13 in esophageal squamous cell carcinoma. Genes Chromosomes Cancer **32:**112–118.
53. **Yoshida, H., T. Matsui, A. Yamamoto, T. Okada, and K. Mori.** 2001. XBP1 mRNA is induced by ATF6 and spliced by IRE1 in response to ER stress to produce a highly active transcription factor. Cell **107:**881–891.
54. **Zou, Z., A. Anisowicz, M. J. Hendrix, A. Thor, M. Neveu, S. Sheng, K. Rafidi, E. Seftor, and R. Sager.** 1994. Maspin, a serpin with tumor-suppressing activity in human mammary epithelial cells. Science **263:**526–529.